CHAPTER SIXTEEN

SPECTRA AND ELECTRONIC STRUCTURES OF FREE ACTINIDE ATOMS AND IONS

Earl F. Worden, Jean Blaise, Mark Fred*,
Norbert Trautmann, and Jean-François Wyart

Dedicated to Mark Fred (1912–1994), John G. Conway (1922–1995), and Frank Tomkins (1915–1999).

* Deceased.

16.1 INTRODUCTION

This chapter reviews the spectra and the deduced electronic properties of isolated actinide atoms and ions observed in the vapor phase at low density. The free atoms or ions have all or most of the valence electrons present, and the observed spectra can be assigned to transitions due essentially to changes in the quantum numbers of the valence electrons. This is in contrast to the spectra of actinides in crystals or in solution (dealt with in depth in Chapter 18), where the observed spectra are largely due to transitions within the 5f shell. In crystals, the actinide ions are exposed to the electric field of the surrounding ions, which produces a Stark effect on the levels. The magnitude of the effect is relatively small because the 5f electrons are shielded from the crystal field by the 6s and 6p electrons. The result is a small perturbation in which each 5f level is split into a number of close components. In free atoms, the valence electrons interact strongly with the 5f electrons and also with each other. Hence each 5f level gives rise to many daughter levels that are more widely split than the parent separations and have large angular momentum contributions from the parent. The result in this case is a great number of levels whose structure is not simply related to the structure of the 5f levels or to the structure of the valence-electron levels by themselves. It is evident that the 5f level structure can be obtained more directly from crystal spectra but the properties of the valence electrons (in particular, implications for the chemical properties) must be deduced from the free-atom spectra.

Historically, the correlation between actinide chemistry and spectroscopy was anticipated before much experimental information was available in either field. Therefore interest in actinide spectroscopy was as an aid to predicting actinide chemistry, in the expectation that smaller quantities of these elements would be required. In practice, the chemistry developed first as soon as sufficient amounts of material were produced, while the spectroscopy encountered difficulties because the complexities were underestimated. The difficulty was not so much as the enormous total number of levels, which could be counted readily, but the extent to which the levels interacted so as to preclude simplification.

The interaction implies that each level is a mixture of various pure states labeled by quantum numbers for the 5f shell and also by quantum numbers for each valence-electron shell. Different levels have different mixtures, and the composition of each level cannot be deduced by inspection because of the large number of quantum numbers, with a different energy dependence for each. Thus the compositions must be derived by comparison with theoretical calculations. The calculations are difficult to perform even with a large computer, and because of the mixing, the results do not give a simple picture of the way in which the energy of an actinide atom depends on the valence-electron configuration. This complexity is inherent in atoms with 5f electrons, and the chemistry is correspondingly more difficult to predict. Nevertheless, it is clearly desirable to attempt it.

We begin with a discussion of some experimental techniques, then present an introduction to the theory, and finally relate the electronic structure obtained from the spectroscopic data to the chemistry of the actinide elements. Laser spectroscopic techniques are discussed, which have improved the quality of isotope shift (IS) and hyperfine structure (hfs) data. These methods have increased the accuracy of the ionization potentials (IPs) of the actinide elements where sufficient (and in some cases only very small) quantities of atoms can be produced. A few new energy levels have been found for Fm and Es by the resonance ionization mass spectroscopy (RIMS) technique, but no new information has been obtained to date on the electronic structure of the heavier actinides (beyond Fm). A discussion of the spectroscopy of deformed isomers of Am is included.

16.2 EXPERIMENTAL SPECTROSCOPY OF FREE ACTINIDE ATOMS AND IONS

The main interest in actinide spectra, besides finding lines useful for chemical analyses of the elements, is in energy level analysis. This methodology determines the relative energies of various electron configurations for each actinide and the way the interactions between different kinds of electrons vary along the actinide series. The first step in this process is to obtain the complete (as possible) spectra for each element. For conventional actinide spectroscopy, the limit is Es, the element with atomic number 99. Thus four elements, Fm to Lw, have little experimental spectroscopic results. Limited beam and laser spectroscopy, plus extrapolation and theory, are all that is available for determining the optical spectra and electronic structure of these four elements.

In each actinide spectrum, tens of thousands of spectral lines are observed and many more are possible but weak. No order is apparent. The determination of the energy levels from the lines is based chiefly on the search for recurrent differences (or sums) between the energies (wavenumbers) of various pairs of lines, indicating pairs of transitions to a given pair of levels from levels of opposite parity. The level structure can be derived in principle by establishing a number of such level pairs. For actinide spectra, a purely numerical approach is not possible for the following reasons:

(1) The large line density usually yields many more fortuitous recurrences than real ones, but improvement in the accuracy of the line list can significantly reduce the number.
(2) The real recurrences due to transitions involving a given pair of levels are limited by selection rules.
(3) The strong lines can often be paired with weak lines that may be too weak to be observed and thus be missed.

Hence one needs to observe the energies of as many lines as possible, measured with the highest accuracy and resolution, as contrasted with spectrochemical analysis, where only a relatively small number of strong lines are required. Corroborative information, such as Zeeman data, ISs, hfs, vapor absorption or self-absorption in an electrodeless discharge lamp (EDL), spectral assignment, is essential.

Experimental techniques have been adequate for the production of neutral (atomic, An I where An represents any actinide element) and first-ion spectra (singly ionized, An II), in spite of the limitations of available sample size and the associated radioactivity for all the actinides up to and including Es. The usual light source is an EDL made from quartz tubing with about 2–3 mm i.d., 5–6 mm o.d., and about 22–25 mm long, into which the sample ($\sim$0.1 mg as anhydrous An iodides) is sublimed. The lamp is then sealed off under vacuum, as described in Tomkins and Fred (1957) and in Worden *et al.* (1963). A microwave discharge supplies the heat to volatilize the sample, and the electron energy to dissociate the molecules and excite the atomic spectrum. This source is sensitive, confines the radioactivity, gives sharp lines, and can be run in a magnetic field. It can also be used to differentiate lines of the neutral spectrum from those of the first ion by observation of the spectrum at high and low microwave powers (or high and low atom density). At very high power or high atom density, self-reversal of lines from the low-lying levels of the neutral atoms, and in some cases the first ion of the element, were observed. The lamps allow complete recovery of the element after use. This is a very important consideration for rare isotopes where the cost of production is high and only limited quantities are available. Unfortunately a comparable source for the higher ions (much higher electron temperature required) is not yet available. A few lines of the third spectrum of some actinides have been observed in special hollow cathode lamps but not from EDLs.

The design and construction of EDLs of Es, when amounts of $\sim$100 mg or more became available, had to be changed because of the poor yields ($<$15%) obtained with no carrier element present (Worden *et al.*, 1968, 1970 and especially Worden *et al.*, 1974). These changes are described in detail in Appendix 16.1.

Initial analyses of all actinide spectra are based on measurements of photographic plates taken on the Argonne National Laboratory (ANL) 9.15 m Paschen-Runge and 3.4 m Ebert spectrographs with high-angle gratings (now decommissioned). These instruments covered a large wavelength range at high resolving power with a single exposure (providing wavenumber (energy) accuracy of 0.02 cm^{-1} or higher (Tomkins and Fred, 1963; Worden and Conway, 1970; Worden *et al.*, 1970, 1974, 1987). Because photographic plates were used, several exposures were required. The plates were measured using semiautomatic comparators with 1 μm accuracy (Tomkins and Fred, 1951). The thorium spectrum was used in order to provide standards to establish the unknown

wavelengths. In the case of the highly radioactive elements, it was essential to remove the lines of the decay products as well as other impurity lines from the line list before beginning the analyses of the spectra. The near-infrared and infrared spectra of the actinide elements were observed with Fourier transform spectrometers (FTSs) (see for example Conway *et al*., 1976). The assembly of an accurate line list and other supporting data suitable for level analysis required 3–6 years. The hfs and IS can be obtained with FTSs, but calibration of the IS data is needed when using separated isotopes in EDLs where there are no internal standard lines for production of a calibrated energy scale (Pulliam *et al*., 2003).

An FTS with comparable resolving power but better energy accuracy (0.005 cm^{-1} or higher) than the ANL spectrograph has been operational at the Laboratoire Aimé Cotton (LAC), Orsay, France, since 1970. Built initially for the infrared region, it covers the region 4000–400 nm (Connes *et al.*, 1970). A second FTS covered the visible and ultraviolet regions down to 345 nm. By 1976, another high-resolution FTS had been built at the National Solar Observatory, Kitt Peak, Arizona (Brault, 1976). All the actinide spectra from Th to Cf have now been recorded with one or more of these instruments. Observation of the infrared spectrum with high resolution and accuracy is especially important for the term analyses of the lanthanide and actinide spectra because of the large number of low-lying energy levels that give transitions in this spectral region. The spectra of a number of actinides have been recorded over the full range ($\sim$1800 to 50 000 cm^{-1}, or because of quartz lamp limitations, 3500–45 000 cm^{-1}) on the 1 m FTS at Kitt Peak.

The advent of atomic vapor laser isotope separation (AVLIS) in the early 1970s stimulated considerable interest in the laser spectroscopy of actinides, primarily on U and other light actinide elements that continues to the present. These efforts involve many countries besides the USA, including Canada, France, England, Germany, Italy, Japan, India, and China. More conventional actinide spectroscopy, in addition to laser spectroscopy, has continued in France and Germany. Blaise and Wyart at LAC are compiling actinide energy levels and extending current analyses and theory for some heavier actinides. German work is based on the low-level detection of actinides, and has resulted in the very accurate determination of actinide IPs, the study of isomer shifts, and recently the finding of a limited number of levels in Es (Peterson *et al*., 1998) and Fm (Sewtz *et al*., 2003) by laser techniques. Complete line lists with level assignments of some of the actinides are now available from the National Institute of Standards and Technology (NIST). Atlases that include scans, line frequencies, and level assignments for FTS observations are available from Los Alamos National Laboratory (LANL) on Th (Palmer and Engleman, 1983) and U (Palmer *et al*., 1980).

The present status of the term analyses of actinide spectra varies from essentially complete for the elements with even atomic number (Th, U, Pu, Cm, and Cf) to partial analyses for some of the odd isotopes. In the first category, nearly

all the strong and moderate-intensity lines have been classified and only weak lines remain to be assigned. However, these are a considerable fraction of the total number. Conventional publication of so much data is impracticable; thus this information is in some cases available only in the laboratory doing the work. Nevertheless, wavelengths of the strongest emission lines of all the actinides from Ac through Cf have been tabulated according to the stage of ionization (Reader and Corliss, 1980). Blaise and Wyart (1992) have published all known energy levels of the actinides analyzed up to that time and list ionization stage, energies, intensities, *J*-values, and level assignments of selected lines of all actinides through Es. The contents of this volume are being transferred and updated on a database at LACs website www.lac.u-psud.fr. Table 16.1 summarizes the lowest determined level for each known configuration of the actinide elements. In some cases, the references in Table 16.1 include extensive line lists of the classified lines and known energy levels.

After a major campaign in 1975–76 to observe the ^{253}Es and ^{250}Cf atomic spectra, the number of workers doing energy-level analyses has steadily decreased worldwide. At the present time only a very few laboratories are pursuing studies of this type.

16.3 EMPIRICAL ANALYSIS OF ACTINIDE SPECTRA

A neutral actinide has typically less than a 1000 known experimental levels, the first ion somewhat fewer, primarily due to the low excitation energy of the EDL source. The levels are organized by half-dozen into terms, some dozens of terms form a configuration, and there are often ten or more configurations identified for a given stage of ionization. The order in this hierarchy, however, is not evident. There is considerable overlapping of different terms and of different configurations. The terms are not pure in any coupling scheme but must be described as mixtures to account for their properties, and there is more often than not mixing of configurations. The only way most levels can be identified with a given configuration is by the use of the observed IS, the intensities of its transitions to levels of known configurations, and by comparison with theoretical calculations with appropriate parameters.

There are several fortunate circumstances that make it possible to identify the lowest level of each configuration and thereby the relative energies of the configurations (for interpretation of the structure). In *SL* coupling the lowest level of a configuration is usually found to be fairly pure and follows Hund's rules, i.e. this term has maximum multiplicity and maximum orbital angular momentum. Fig. 16.1 shows, as an example of Hund's rules, the lowest term of a number of configurations in neutral plutonium. Although Hund's rules apply only in configurations of equivalent electrons, they are followed, with few exceptions, in configurations with several open subshells.

Table 16.1 *Lowest levels found for identified configurations, with parity, terms, IS values, and hfs widths* (*Widths are negative for inverted hfs splitting*). *Under configuration all have the radon core as part of the configuration. Under references, the first initial of all authors plus the date gives the reference. A question mark means the data are missing or in question.*

Spectrum measured isotopes	*Configuration*	*Parity/term*		*Level* (cm^{-1})	g_{obs}	*IS* (10^{-3} cm^{-1})	*hfs* (10^{-3} cm^{-1})	*References*[a]
Ac III	7s	E	$^2S_{1/2}$	0.0				Meggers *et al.* (1957)
	6d	E	$^2D_{3/2}$	801.0				
	5f	O	$^2F_{5/2}$	23 454.5				
	7p	O	$^2P_{1/2}$	29 465.9				
Ac II	$7s^2$	E	$^1S_0$	0.00				Meggers *et al.* (1957)
	6d7s	E	$^3D_1$	4739.63				Klinkenberg and Lang (1949)
	$6d^2$	E	$^3F_2$	13 236.46				
	7s7p	O	$^3P_0$	20 956.40				
	6d7p	O	$^3P_2$	26 446.96				
	5f7s	O	$^3F_2$	31 878.87				
	5f6d	O	$^3H_4$	39 807.14				
	7s8s	E	$^3S_1$	51 680.55				
	5f7p	E	$^3F_2$	54 633.05				
Ac I	$6d7s^2$	E	$^2D_{3/2}$	0.00				Meggers *et al.* (1957)
	$6d^27s$	E	$^4F_{3/2}$	92 17.28				
	$7s^27p$	O	$^2P_{1/2}$	?				
	6d7s7p	O	$^4F_{3/2}$	13 712.90				
	$6d^27p$	O	$^4G_{5/2}$	31 494.68				
Th IV	5f	O	$^2F_{5/2}$	0.00				Klinkenberg and Lang (1949)
232	6d	E	$^2D_{3/2}$	9193.245				Klinkenberg (1988)
	7s	E	$^2S_{1/2}$	23 130.75				
	7p	O	$^2P_{1/2}$	60 239.10				
	8s	E	$^2S_{1/2}$	119 621.60				
	7d	E	$^2D_{3/2}$	119 684.60				
	6f	O	$^2F_{5/2}$	127 269.2				

	8p	O	$^2P_{1/2}$	134 516.50				
	5g	E	$^2G_{9/2}$	159 371.				
	9s	E	$^2S_{1/2}$	160 728.1				
	8d	E	$^2D_{3/2}$	161 954.				
	7f	O	$^2F_{5/2}$	164 554.7				
	6g	E	$^2G_{9/2}$	181 674.				
	10s	E	$^2S_{1/2}$	182 441.				
Th III	5f6d	O	$^3H_4$	0.000	0.89			Klinkenberg (1950)
232	$6d^2$	E	$^3F_2$	63.267	0.744			Litzen (1974)
	5f7s	O	$^3F_3$	2527.095	1.071			Wyart and Kaufman (1981)
	6d7s	E	$^3D_1$	5523.881	0.50			Klinkenberg and Uylings (1986)
	$7s^2$	E	$^1S_0$	15 148.519	0.81			
	5f7p	E	$^3G_3$	33 562.349	0.849			
	6d7p	O	$^3F_2$	37 280.229	0.793			
	7s7p	O	$^3P_0$	42 259.714				
	5f8s	O	$J = 2$	74 644.27				
	5f7d	O	$J = 3$	78 327.71				
	6d8s	E	$^3D_1$	81 706.37				
	6d7d	E	$J = 1$	83 358.66				
	5f8p	E	$J = 3$	86 086.37				
	5f6f	E	$J = 5$	86 933.97				
	6d6f	O	$J = 4$	94 657.94				
Th II	$6d^27s$	E	$^4F_{3/2}$	0.000	0.639	0	–141	Zalubas and Corliss (1974)
232	$6d7s^2$	E	$^2D_{3/2}$	1859.938	0.586	34	–102	Giacchetti *et al.* (1974)
IS	$5f7s^2$	O	$^2F_{5/2}$	4490.256	0.856	–554	17	Engleman and Palmer (1984)
232–230	5f6d7s	O	$^4H_{7/2}$	6168.351	0.718	–371		
hfs	$6d^3$	E	$^4F_{3/2}$	7001.425	0.800	–422		
229	$5f6d^2$	O	$^4H_{7/2}$	12 485.688	0.855	–680		
	6d7s7p	O	$^4F_{3/2}$	23 372.582	1.067	–554		
	$5f^27s$	E	$^4H_{7/2}$	24 381.802	0.70	–590		
	5f7s7p	E	$^4G_{5/2}$	26 488.644	0.776	–305		
	$6d^27p$	O	$^4G_{5/2}$	28 243.812	0.922	–421		
	5f6d7p	E	$^4I_{9/2}$	30 452.723	1.035	–640		

Table 16.1 (*Contd.*)

Spectrum measured isotopes	*Configuration*	*Parity/term*	*Level* (cm^{-1})	g_{obs}	*IS* (10^{-3} cm^{-1})	*hfs* (10^{-3} cm^{-1})	*References*[a]
	$7s^2 7p$	O $^2P_{1/2}$	31 625.680	0.344	–139		
	$5f^2 6d$	E $^4K_{11/2}$	32 620.859	0.826	–948		
Th I	$6d^2 7s^2$	E $^3F_2$	0.000	0.736	0		Zalubas (1975)
232	$6d^3 7s$	E $^5F_1$	5563.143	0.065	–328		Palmer and Engleman (1983)
IS	$5f6d7s^2$	O $^3H_4$	7795.270	0.863	–244		Engleman and Palmer (1983)
232–230	$6d7s^2 7p$	O $^3F_2$	10 783.153	0.732	–33		Blaise *et al.* (1988a)
	$6d^2 7s7p$	O $^5G_2$	14 465.220	0.810	–209		
	$5f6d^2 7s$	O $^5H_3$	15 618.985	0.600	–535		
	$5f7s^2 7p$	E $^3G_3$	18 431.685		–162		
	$6d^4$	E $^5D_0$	21 176.012		–655		
	5f6d7s7p	E $^5I_4$	22 098.187	0.742	–484		
	$5f^2 7s^2$	E $^3H_4$	27 495.589	1.005	–396		
	$5f6d^3$	O $^5I_4$	31 194.705	0.735	–789		
	$6d^3 7p$	O $^5G_2$	32 575.421	0.720	–672		
	$5f6d^2 7p$	E $^5K_5$	35 300.914	0.875	–671		
Pa II	$5f^2 7s^2$	E $^3H_4$	0.00	0.8212		0	Giacchetti (1967)
231	$5f^2 6d7s$	E $^5K_5$	823.265			–1410	Giacchetti and Blaise (1970)
hfs	$5f6d^2 7s$	O $^5I_4$	4751.660			–1065	
231	$5f6d7s^2$	O $^3H_4$	7312.695			–130	
	$5f^2 6d^2$	E $^5L_6$	7454.030	0.77		205	
	$5f^3 6d$	O $^5L_6$?	19 162.305			315	
	$5f^2 7s7p$	O $^5I_4$	22 549.535?			–680	
Pa I	$5f^2 6d7s^2$	E $^4K_{11/2}$	0.000	0.820		0	Giacchetti (1966)
231	$5f6d^2 7s^2$	O $^4H_{7/2}$	1978.220	0.790		–130	Blaise and Giacchetti (1970)
hfs	$5f^2 6d^2 7s$	E $^6L_{11/2}$	7000.290			–1030	Blaise *et al.* (1985)
231	$5f6d^3 7s$	O $^6I_{7/2}$	7585.025			–585	
	$5f^2 7s^2 7p$	O $^4I_{9/2}$	11 444.705	0.88		145	

	$5f^3 7s^2$	O	$^4I_{9/2}$	13 018.610	0.81		–100	
	$5f6d7s^2 7p$	E	$^4I_{9/2}$	14 227.130?	0.980		–155	
	$5f^2 6d7s7p$	O	$^6L_{11/2}$	14 393.410	0.675		–745	
	$5f6d^2 7s7p$	E	$^6I_{7/2}$	15 061.150			–705	
	$5f^2 6d^2 7p$	O	$^6M_{13/2}$	25 106.985	0.980		–310	
U VI	5f	O	$^2F_{5/2}$	0.0				Kaufman and Radziemski (1976)
238	6d	E	$^2D_{3/2}$	90 999.6				
	7s	E	$^2S_{1/2}$	141 447.5				
	7p	O	$^2P_{1/2}$	193 340.2				
U V	$6p^6 5f^2$	E	$^3H_4$	0.00				Wyart *et al.* (1980)
238	$6p^6 5f6d$	O	$^3H_4$	59 183.36				Van Deurzen *et al.* (1984)
	$6p^6 5f7s$	O	$^3F_2$	94 069.53				
	$6p^6 6d^2$	E	$^3F_2$	137 608.14				
	$6p^6 5f7p$	E	$^3G_3$	139 140.96				
	$6p^5 5f^3$	E	$J = 4$	145 870.70				
U III	$6p^6 5f^4$	E	$^5I_4$	0.000		0		Blaise *et al.* (1984)
238	$6p^6 5f^3 6d$	O	$^5L_6$	210.265		291		Blaise *et al.* (1987)
IS	$6p^6 5f^3 7s$	O	$^5I_4$	3743.963		1340		
238–235	$5f^2 6d^2$	E	$^5L_6$	19 416.772		719		
	$5f^3 7p$	E	$^5K_5$	36 651.404		824		
U II	$5f^3 7s^2$	O	$^4I_{9/2}$	0.000	0.765	0		Steinhaus *et al.* (1971)
238	$5f^3 6d7s$	O	$^6L_{11/2}$	289.040	0.655	–788		Blaise *et al.* (1980)
IS	$5f^3 6d^2$	O	$^6M_{13/2}$	4585.434	0.785	–1286		Palmer *et al.* (1980)
238–235	$5f^4 7s$	E	$^6I_{7/2}$	4663.803	0.480			Conway *et al.* (1984)
	$5f^4 6d$	E	$^6L_{11/2}$	12 513.885	0.680			Blaise *et al.* (1994)
	$5f^2 6d^2 7s$	E	$^6L_{11/2}$	13 783.030	0.685			
	$5f^2 6d7s^2$	E	$^4K_{11/2}$	17 434.364?	0.795			
	$5f^3 7s7p$	E	$^6K_{9/2}$	23 315.090	0.880			
	$5f^3 6d7p$	E	$^6M_{13/2}$	26 191.309	0.890			
	$5f^4 7p$	O	$^6K_{9/2}$	30 599.179	0.900			
U I	$5f^3 6d7s^2$	O	$^5L_6$	0.000	0.750	0	–112	Steinhaus *et al.* (1971)
238	$5f^3 6d^2 7s$	O	$^7M_6$	6249.029	0.625	–565		Blaise and Radziemski (1976)
IS	$5f^4 7s^2$	E	$^5I_4$	7020.710	0.660	–310		Rajnak (1979)

Table 16.1 (*Contd.*)

Spectrum measured isotopes	*Configuration*	*Parity/term*	*Level* (cm^{-1})	g_{obs}	*IS* (10^{-3} cm^{-1})	*hfs* (10^{-3} cm^{-1})	*References*[a]
238–235	$5f^26d^27s^2$	E $^5L_6$	11 502.624	0.775	450		Childs *et al.* (1979a,b)
hfs 235	$5f^37s^27p$	E $^5K_5$	11 613.975	0.740	175		Engleman and Palmer (1980)
	$5f^36d7s7p$	E $^7M_6$	14 643.867	0.675	–380		Palmer *et al.* (1980)
	$5f^46d7s$	E $^7L_5$	14 839.736	0.565	–380		Conway (1984)
	$5f^47s7p$	O $^7K_4$	22 792.372	0.645	–665		
	$5f^36d^3$	O $^7M_6$	23 084.307?	0.825	–699?		
	$5f^26d^27s7p$	O $7M_7$?	27 576.161	0.99	–170		
	$5f^36d^27p$	E $7N_7$	27 886.992	0.850	–580		
	$5f^37d7s^2$	O $^5L_6$	27 920.942	0.835	40		
	$5f^36d7s8s$	O $^7L_5$	32 857.449	0.760	–360		
	$5f^36d7s8p$	E $^7M_6$	33 639.562	0.820	–420		
	$5f^46d7p$	O $^7M_6$	34 160.569	0.890	–770		
Np II	$5f^46d7s$	E $^7L_5$	0.000			–1722	Fred *et al.* (1976)
237	$5f^47s^2$	E $^5H_4$	24.270	0.650		776	Blaise *et al.* (1977)
hfs 237	$5f^57s$	O $^7H_2$	83.490			–1585	Blaise *et al.* (1980)
	$5f^56d$	O $^7K_4$	9446.880	0.485		936	
	$5f^47s7p$	O $J = 4$	21 922.530			–528	
	$5f^57p$	E $J = 4$	22 720.500			670	
Np I	$5f^46d7s^2$	E $^6L_{11/2}$	0.000	0.655		777	Fred *et al.* (1977)
237	$5f^57s^2$	O $^6H_{5/2}$	2831.140	0.43		534	Blaise *et al.* (1980)
hfs 237	$5f^46d^27s$	E $^8M_{11/2}$	7112.430	0.48		–924	
	$5f^47s^27p$	O $^6K_{9/2}$	11 940.075	0.625		976	
	$5f^56d7s$	O $^8K_{7/2}$	13 384.205			–1008	
	$5f^46d7s7p$	O $^8M_{11/2}$	14 338.880			–661	
	$5f^57s7p$	E $^8I_{5/2}$	18 654.895	0.71		75	
	$5f^36d^27s^2$	O $^6M_{13/2}$	20 050.905	0.780		842	
	$5f^46d^27p$	O $^8N_{13/2}$	28 551.035	0.940		1183	

	$5f^4 7s7p^2$	E	$^8K_{7/2}$	32 896.360	0.86		467	
Pu II	$5f^6 7s$	E	$^8F_{1/2}$	0.000	3.150	381		McNally and Griffin (1959)
240	$5f^5 7s^2$	O	$^6H_{5/2}$	8198.665	0.414	896		Bauche *et al.* (1963a,b)
IS	$5f^5 6d7s$	O	$^8K_{7/2}$	8709.640	0.308	555		Bauche-Arnoult *et al.* (1973)
240–239	$5f^6 6d$	E	$^8H_{3/2}$	12 007.503	–0.019	77		Blaise *et al.* (1980)
hfs 239	$5f^5 6d^2$	O	$^8L_{9/2}$	17 296.880	0.494	242		Blaise *et al.* (1983)
	$5f^6 7p$	O	$^8G_{1/2}$	22 038.950	0.345	287		
	$5f^5 7s7p$	E	$^8I_{5/2}$	30 956.355	0.646	424		
	$5f^5 6d7p$	E	$^8L_{9/2}$	33 793.295	0.800	208		
	$5f^4 6d^2 7s$	E	$^8M_{11/2}$	37 640.775	0.70	813		
Pu I	$5f^6 7s^2$	E	$^7F_0$	0.000		465		Blaise *et al.* (1962)
240	$5f^5 6d7s^2$	O	$^7K_4$	6313.866	0.487	653		Bauche *et al.* (1963a,b)
IS	$5f^6 6d7s$	E	$^9H_1$	13 528.246	–0.59	253		Blaise *et al.* (1980)
240–239	$5f^5 6d^2 7s$	O	$^9L_4$	14 912.011	0.496	488		Striganov (1983
	$5f^6 7s7p$	O	$^9G_0$	15 449.475		336		Blaise *et al.* (1984b)
	$5f^5 7s^2 7p$	E	$^7I_3$	17 897.917	0.450	691		Blaise *et al.* (1986)
	$5f^5 6d7s7p$	E	$^9L_4$	20 828.475	0.352	467		
	$5f^7 7s$	O	$^9S_4$	25 192.231	1.768	273		
	$5f^6 7s8s$	E	$^9F_1$	31 572.610	2.403	446		
	$5f^6 6d^2$	E	$^9I_2$	31 710.912	0.200	115		
	$5f^6 6d7p$	O	$^9I_2$	33 070.577	0.673	293		
	$5f^4 6d^2 7s^2$	E	$^7M_6$	36 050.520	0.850	535		
	$5f^5 6d^2 7p$	E	$^9M_5$	37 415.495	0.980	403		
	$5f^5 6d7s8s$	O	$^9K_3$	39 618.178	0.27	503		
Am II	$5f^7 7s$	O	$^9S_4$	0.00		400	1726	Fred and Tomkins (1957)
241	$5f^7 6d$	O	$^9D_3$	14 222.21		–17	–260	
IS 243–241	$5f^6 6d7s$	E	$J = 2$	20 501.00		547	–929	
hfs 241	$5f^7 7p$	E	$^9P_3$	23 117.18		507	1084	
Am I	$5f^7 7s^2$	O	$^8S_{7/2}$	0.000	1.937	0	–11	Fred and Tomkins (1957)
241	$5f^6 6d7s^2$	E	$^8H_{3/2}$	10 683.568		268	83	Marrus *et al.* (1960)
IS 243–241	$5f^7 6d7s$	O	$^{10}D_{5/2}$	14 506.922		–269	1021	Blaise *et al.* (1980)
hfs 241	$5f^7 7s7p$	E	$^{10}P_{7/2}$	15 608.260	1.382	–210	933	Pulliam (1985)
	$5f^6 6d^2 7s$	E	$^{10}I_{3/2}$	20 522.51				Pulliam *et al.* (2003)

Table 16.1 (*Contd.*)

Spectrum measured isotopes	*Configuration*	*Parity/term*	*Level* (cm^{-1})	g_{obs}	*IS* (10^{-3} cm^{-1})	*hfs* (10^{-3} cm^{-1})	*References*[a]
	$5f^6 7s^2 7p$	O $^8G_{1/2}$	22 860.445				
	$5f^6 6d7s7p$	O $^{10}I_{3/2}$	25 876.47		–17		
	$5f^7 7s8s$	O $^{10}S_{9/2}$	30 884.995		–130	1859	
	$5f^7 6d^2$	O $^{10}F_{3/2}$	33 972.03		–520		
Cm II	$5f^7 7s^2$	O $^8S_{7/2}$	0.00	1.935	0		Worden and Conway (1967)
244	$5f^8 7s$	E $^8F_{13/2}$	2093.870	1.500	–738		Conway *et al.* (1976)
IS	$5f^7 6d7s$	O $^{10}D_{5/2}$	4010.645	2.492	–496		Worden *et al.* (1976a)
246–244	$5f^7 6d^2$	O $^{10}F_{3/2}$	14 830.150	3.009	–962		Blaise *et al.* (1980)
	$5f^8 6d$	E $^8G_{13/2}$	17 150.790	1.415	–1177		Blaise *et al.* (1981)
	$5f^7 7s7p$	E $^{10}P_{7/2}$	24 046.385	2.098	–403		Worden *et al.* (1986)
	$5f^8 7p$	O $^8F_{11/2}$	27 065.085	1.51	–972		
	$5f^7 6d7p$	E $^{10}F_{3/2}$	32 034.430	2.933	–923		
Cm I	$5f^7 6d7s^2$	O $^9D_2$	0.000	2.563	0		Conway *et al.* (1976)
244	$5f^8 7s^2$	E $^7F_6$	1214.203	1.452	–275		Worden *et al.* (1976a)
IS 246–244	$5f^7 7s^2 7p$	E $^9P_3$	9263.374	2.112	118		Lobikov *et al.* (1979)
	$5f^7 6d^2 7s$	O $^{11}F_2$	10 144.927	2.873	–339		Worden and Conway (1976b)
	$5f^7 6d7s7p$	E $^{11}F_2$	15 252.710	2.835	–269		Blaise *et al.* (1980)
	$5f^8 6d7s$	E $^9G_7$	16 932.750	1.466	–586		Worden *et al.* (1985)
	$5f^8 7s7p$	O $^9D_6$	17 656.657	1.621	–463		Blaise *et al.* (1988b)
	$5f^7 7s^2 8s$	O $^9S_4$	28 635.020	1.731	–126		
	$5f^7 6d^3$	O $^{11}F_2$	30 443.915	2.53	–619		
	$5f^7 7s7p^2$	O $^{11}P_4$	31 167.969	1.759	–180		
	$5f^8 6d7p$	O $^9H_8$	32 876.853		–720		
	$5f^8 7s8s$	E $^9F_7$	33 013.035	1.54	–450		
	$5f^7 6d7s8s$	O $^{11}D_3$	34 255.170	2.064	–220		
	$5f^7 6d^2 7p$	E $J = 5$	34 290.497	1.466	–526		
	$5f^7 7s^2 8p$	E $^9P_3$	35 540.695	2.00	135		

	$5f^8 6d7p$	O	$J = 7$	35 694.690	1.358	–677		
	$5f^7 7d7s^2$	O	$^9D_2$	36 481.435	2.373	105		
	$5f^8 7p^2$	E	$^9F_6$	37 631.966	1.48	–813		
	$5f^8 7s8p$	O	$J = 6$	38 092.623	1.47	–435		
Bk II	$5f^9 7s$	O	$^7H_8$	0.00			6195	Worden *et al.* (1967)
249	$5f^8 7s^2$	E	$^7F_6$	7040.98			820	Conway *et al.* (1977a)
hfs 249	$5f^8 6d7s$	E	$J = 8$	12 340.96			8678	Worden and Conway (1978)
	$5f^9 6d$	O	$J = 8$	16 360.00			670	Blaise *et al.* (1980)
	$5f^9 7p$	E	$J = 7$	26 938.26			2050	Worden *et al.* (1987)
	$5f^8 7s7p$	O	$J = 6$	32 025.72			3445	
Bk I	$5f^9 7s^2$	O	$^6H_{15/2}$	0.00	1.28		1150	Worden *et al.* (1967)
249	$5f^8 6d7s^2$	E	$^8G_{13/2}$	9141.115	1.415		836	Conway *et al.* (1977a)
hfs 249	$5f^9 7s7p$	E	$J = 15/2$	16 913.770			3168	Worden and Conway (1978)
	$5f^9 6d7s$	O	$J = 17/2$	17 182.482			4472	Blaise *et al.* (1980)
	$5f^8 7s^2 7p$	O	$J = 11/2$	17 777.808			157	Worden *et al.* (1987)
	$5f^8 6d^2 7s$	E	$^{10}G_{13/2}$	21 506.406	1.550		3596	
	$5f^8 6d7s7p$	O	$J = 13/2$	24 652.405	1.38		1157	
	$5f^9 7s8s$	O	$^8H_{17/2}$	32 488.850			6306	
	$5f^9 6d7p$	E	$J = 17/2$	36 952.610			1800	
Cf II	$5f^{10} 6s$	E	$^6I_{17/2}$	0.00	1.28			Worden and Conway (1970)
249	$5f^{10} 6d$	E	$J = 15/2$	19 359.06				Conway *et al.* (1977a)
hfs 249	$5f^9 6d7s$	O	$J = 19/2$	24 213.34	1.27			Blaise *et al.* (1980)
	$5f^{10} 7p$	O	$J = 15/2$	26 858.90	1.26			Conway *et al.* (1995)
Cf I	$5f^{10} 7s^2$	E	$^5I_8$	0.000	1.213		0	Worden and Conway (1970)
249	$5f^9 6d7s^2$	O	$J = 8$	16 909.355	1.301		–40	Conway *et al.* (1977a)
hfs 249	$5f^{10} 7s7p$	O	$J = 8$	17 459.210	1.277		–140	Blaise *et al.* (1980)
	$5f^{10} 6d7s$	E	$J = 8$	20 043.930			–210	Conway *et al.* (1995)
	$5f^9 7s^2 7p$	E	$J = 7$	24 727.600			60	
	$5f^{10} 7s8s$	E	$^7I_9$	32 983.180	1.300		–490	
	$5f^9 6d7s7p$	E	$J = 8$	33 952.135			–200	
	$5f^{10} 7s8p$	O	$J = 8$	38 225.945			–410	
	$5f^{10} 7s7d$	E	$J = 8$	39 081.175	1.245			
	$5f^9 7s^2 8s$	O	$J = 8$	45 183.155			–150	

Table 16.1 (*Contd.*)

Spectrum measured isotopes	*Configuration*	*Parity/term*		*Level* (cm^{-1})	g_{obs}	*IS* (10^{-3} cm^{-1})	*hfs* (10^{-3} cm^{-1})	*References*[a]
Es II	$5f^{11}7s$	O	$^5I_8$	0.00			7086	Gutmacher *et al.* (1967)
253	$5f^{11}6d$	O	$J = 7?$	21 639.58			1250	Worden *et al.* (1970)
hfs 253	$5f^{11}7p$	E	$J = 7$	27 751.12			442	Worden *et al.* (1974)
								Blaise *et al.* (1980)
								Blaise *et al.* (2003)
Es I	$5f^{11}7s^2$	O	$^4I_{15/2}$	0.00	1.185		1543	Worden *et al.* (1968)
253	$5f^{11}7s7p$	E	$J = 15/2$	17 802.87			3838	Worden *et al.* (1974)
hfs 253	$5f^{10}6d7s^2$	E	$J = 15/2$	20 162.56			1550	Blaise *et al.* (1980)
	$5f^{11}7s8s$	O	$^6I_{17/2}$	33 829.35			6280	Blaise *et al.* (2003)
	$5f^{10}6d7s7p$	O	$J = 15/2$	37485.58			3870	Wyart *et al.* (2005)
	$5f^{11}7s7d$	O	$J = 13/2$	40478.25			6557	Wyart *et al.* (2005)

[a] Complete energy levels etc. of all the atoms and ions in this table are given in BW92.

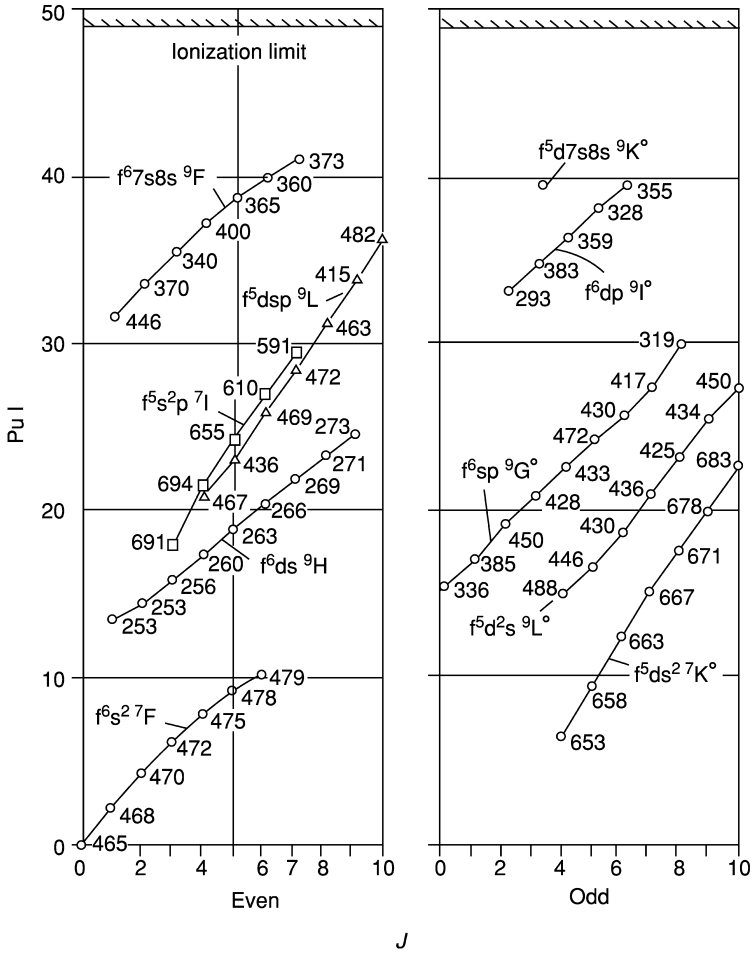

Fig. 16.1 *Hund's rule multiplet of various electron configurations of neutral plutonium,* Pu(*I*). *The number opposite each fine-structure level is the observed isotope shifts* (^{240}Pu–^{239}Pu) *in* 10^{-3} cm^{-1}.

One of the most useful types of experimental corroboration can be obtained from IS values. In the heavy elements the difference in energy of an atomic level from one isotope to another is due to the difference in nuclear volume between the isotopes. For an electron very near the center of the atom, the Coulomb attraction is decreased from that for a point nucleus. The effect is greater for heavier (larger) isotopes. The IS is also greater for electron configurations with more s-electrons since s-electrons have (nonrelativistically) a finite electron

density at the nucleus. The IS is therefore larger for the $5f^n7s^2$ configuration than for the $5f^n7s7p$ configuration. The size of the shift is not directly proportional to the number of 7s electrons because the total s-electron density at the nucleus is modified by the mutual shielding among the electrons. If two 7s electrons are present, the inner electron density of one to some extent shields the outer density of the other from the nuclear attraction, and consequently the $7s^2$ central density is less than twice that for $7s^1$. The presence of an inner electron (5f or, somewhat less so, 6d) also shields a 7s electron. So converting a 5f to a 6d electron reduces the shielding of the 7s electron and increases the IS. Nonrelativistic Hartree–Fock (HF) calculations (Wilson, 1968) gave the result that in converting from one type of valence electron to another, the 5s and 6s electron densities also changed appreciably and had to be considered since it is the total density of all the s-electrons that is responsible for the IS. Relativistic HF calculations (Rajnak and Fred, 1977), on the other hand, ascribe the shift to changes in the shielding of just the 7s electron. Fig. 16.2 shows the experimental shifts and calculated densities at the nucleus for a number of Pu I configurations, illustrating the linear relationship. The experimental shifts are also given for the fine-structure levels of the terms plotted in Fig. 16.1, showing that there is a sensibly constant shift within each set of levels. They are, in fact, fairly constant not only within the lowest term, but also for all the levels of a configuration. The fluctuation is evidently due to varying amounts of configuration interaction (CI), which mixes different configurations and hence mixes the shifts in proportion. The IS values thus make it possible to assign many experimental levels to a definite configuration, which is a very valuable property even though it says nothing about the assignment of term quantum numbers to individual levels within a configuration.

16.4 ELECTRONIC CONFIGURATIONS OF ACTINIDES, SYSTEMATICS OF ACTINIDE CONFIGURATIONS, AND RELATION TO CHEMISTRY

Electron configurations, analogous to the Pu configurations shown in Fig. 16.1, occur in the other actinide elements, i.e. configurations with the same combination of valence electrons but with the number of 5f electrons increasing as Z, the atomic number, increases. These can be generalized into various series, such as $5f^n7s^2$, $5f^{n-1}6d7s^2$, etc., where for the neutral atom $n = Z-88$. Within a series, the S and L of the Hund's rules term change from series member to member because of the changing contribution from the 5f shell. There are also corresponding series for the ions, e.g. $5f^n7s$, $5f^{n-1}6d7s$.

The usefulness of the series concept comes from the regularity in energy of the lowest term. The relative energies of different series change with Z but the change is systematic. This is illustrated in Fig. 16.3(a) and (b) for the neutral

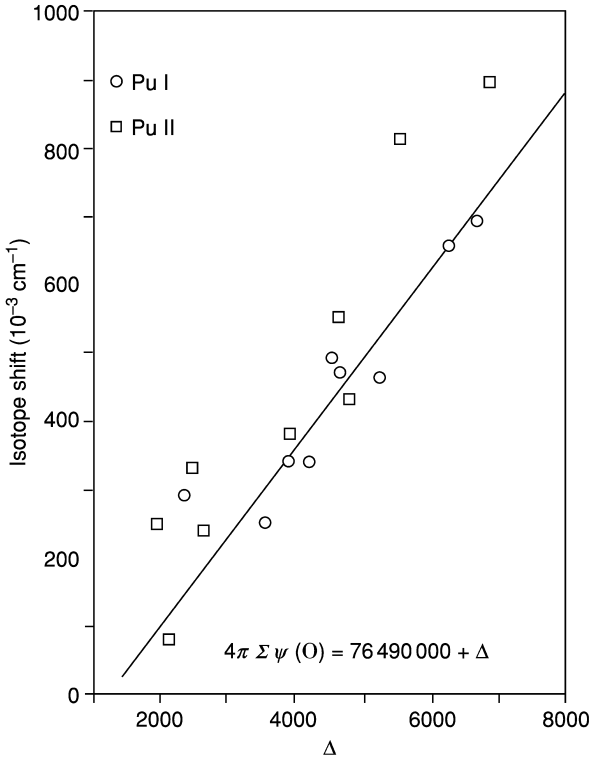

Fig. 16.2 *Isotope shifts of configurations of Pu I and Pu II as a function of electron density at the nucleus.*

atoms; the data are given in Tables 16.1 and 16.2. The absolute binding energies increase with Z (become more negative), but the quantity of interest is usually the relative energy between series. In Fig. 16.3(a) the zero energy for each element has been taken arbitrarily as the configuration $5f^{n-1}6d7s^2$ (the lowest with three valence electrons, trivalent) and in Fig. 16.3(b) the lowest configuration is taken as $5f^n7s^2$ (divalent). The regularity provides independent evidence of the correct assignment of levels to the various series for the individual actinide elements, except for the irregular behavior near the middle of the 5f shell.

This irregularity is due mainly to the fact that the overall spread in energy of the f^n configurations is greatest for the half-filled shell, $n = 7$. (Each f^n configuration consists of a number of SL terms due to the 5f–5f repulsion, and these terms have quite different energies.) Fig. 16.4 shows the approximate position of the lowest term of each f^n configuration with respect to the weighted average of the configuration, and also with respect to the lowest term of f^{n-1}. When f^n is

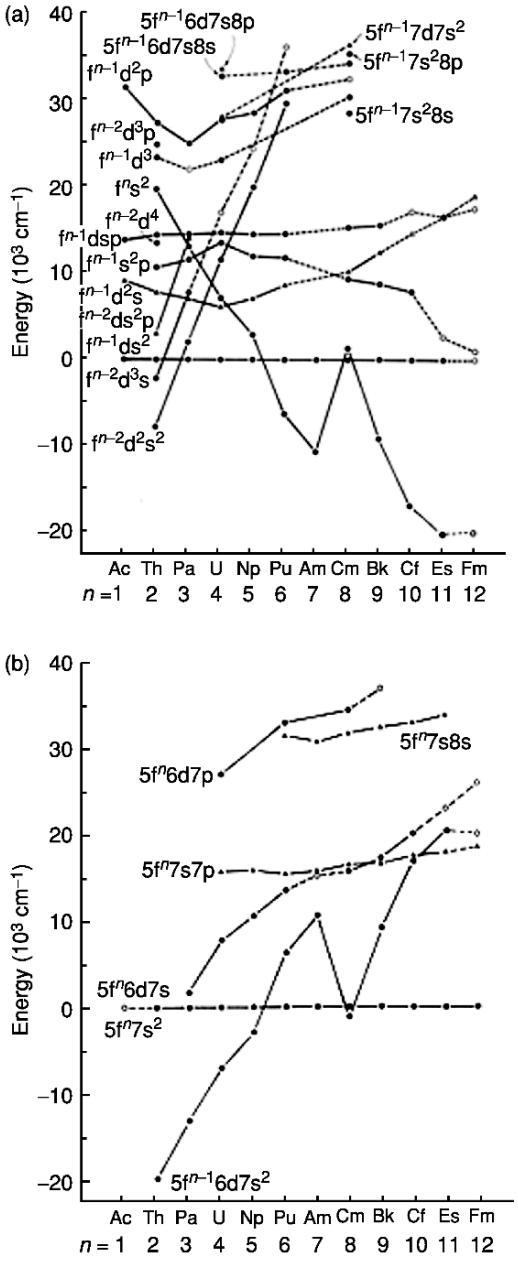

Fig. 16.3 *Energies of various series of configurations in the neutral actinides compared to* $5f^{n-1}6d7s^2$ (*a*) *and* $5f^n7s^2$ (*b*). *The open circles indicate estimates from Brewer* (1971a,b, 1984).

Table 16.2 *Lowest levels of some common configurations of the neutral actinide elements.*

	Ac (*Z* = 89, *N* = 1)	*Th* (90, 2)	*Pa* (91, 3)	*U* (92, 4)	*Np* (93, 5)	*Pu* (94, 6)	*Am* (95, 7)	*Cm* (96, 8)	*Bk* (97, 9)	*Cf* (98, 10)	*Es* (99, 11)	*Fm* (100, 12)	*Md* (101, 13)
$5f^{n-1}6d7s^2$	0	7795	0	0	0	6314	10 684	0	9141	16 909	20 163	(20 000)	(30 000)
$5f^{n-1}6d^27s$	9217	15 619	7000	6249	7112	14 912	20 523	10 145	21 506	(31 500)	(36 000)	(39 000)	(51 000)
$5f^{n-1}7s^27p$	(9500)	18 432	11 445	11 614	11 940	17 898	22 860	9263	17 778	24 728	(22 000)	(21 000)	(28 000)
$5f^{n-1}6d7s7p$	13 713	22 098	14 393	14 644	14 339	20 828	25 876	15 253	24 652	33 952	(36 000)	(37 500)	(48 000)
$5f^n7s^2$	(30 000)	27 496	13 019	7021	2831	0	0	1214	0	0	0	0	0
$5f^n6d7s$	(42 000)	(39 000)	14 693	14 840	13 384	13 528	14 507	16 933	17 182	20 044	(23 000)	(26 000)	(28 000)
$5f^n6d^2$	(59 000)	(57 000)	(39 000)	(34 000)	(27 000)	31 711	33 972	(41 000)	(45 000)	(50 000)	(54 000)	(58 000)	(62 000)
$5f^n7s7p$	(43 000)	(42 000)	(25 600)	22 792	18 655	15 449	15 608	17 657	16 914	17 459	17 803	(18 500)	(19 000)
$5f^{n-2}6d^27s^2$		0	1978	11 503	20 050	36 050	(51 000)	(50 000)					
$5f^{n-2}6d^37s$		5563	7585	(16 930)	(24 500)	(42 500)							

Values in parenthesis are estimates taken from Brewer (1984).

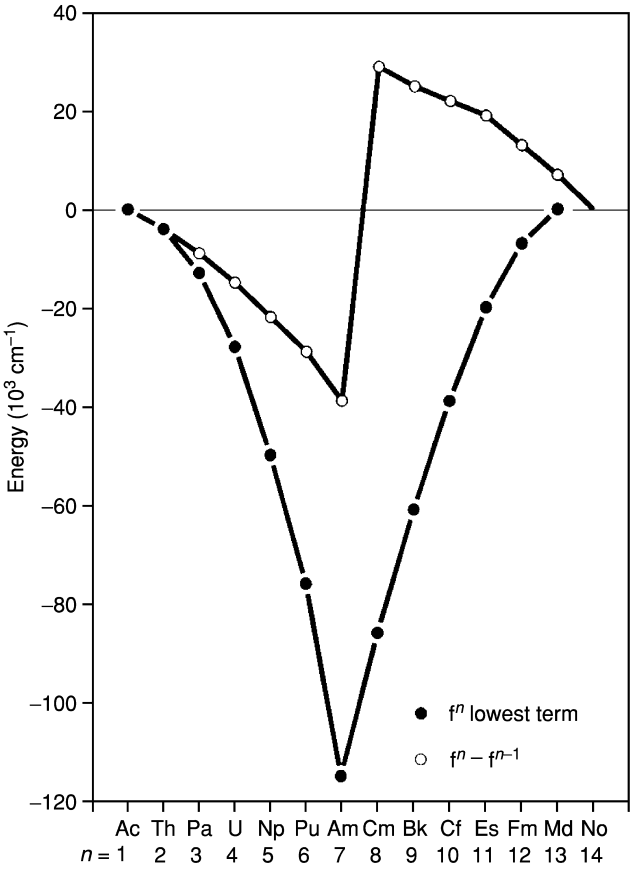

Fig. 16.4. *Approximate energy of the lowest term of f^n relative to the weighted average of f^n and of f^{n-1}.*

compared with $f^{n-1}d$ (the $7s^2$ electrons do not contribute to the structure), the irregularity is reduced because the f–d electrostatic interaction changes sign at $n = 8$, and also slope.

Inspection of Fig. 16.3(a) shows three families of series based on f^n, f^{n-1}, and f^{n-2} having respectively negative, zero, and positive slope. The relative positions of different series characterized by various configurations of outer electrons tend to repeat for each family, and consequently the existence of families is clearly due to the properties of the 5f electrons. For simplicity, Fig. 16.4 presents the lowest series of each family, those configurations with $7s^2$. Now HF calculations show that most of the energy in actinide configurations comes from the electrostatic attraction between the individual 5f electrons and the nucleus. This

attraction increases with Z (the actinide contraction) and the total of the 5f attraction energy is proportional to the number of 5f electrons. The $7s^2$ energy is nearly constant with Z and so does not affect the trend of the series. The 6d energy is also nearly constant but gives an additional (almost constant) contribution to $5f^{n-1}6d7s^2$ and twice as much to $5f^{n-2}6d^27s^2$; it affects the absolute positions of the three series but not the slopes (see Fig. 16.3a). The three series have roughly equal energies for atomic numbers around that of uranium ($Z = 92$). For smaller Z, the 6d binding energy is more important than the 5f binding energy, but for larger Z the 5f becomes increasingly more stable due to an increase with both Z and n.

The electron–nucleus attraction energy is related by the virial theorem to the mean value of r (the electron–nucleus separation) for the different kinds of electrons. Fig. 16.5 shows (nonrelativistic) HF solutions for the radial distribution $P(r)$ for plutonium as a typical actinide. The abscissa is chosen as $r^{1/2}$ (in atomic units) in order to show more detail at small r and less at large r. The figure also shows the total electron density due to the first 86 electrons in the radon core, plotted to a reduced ordinate scale. At the bottom of the figure is Z^*, the effective Z, which describes how the nuclear charge seen by an electron at separation r is reduced by the shielding due to the electron density between zero and r. The 5f electrons clearly see a larger Z^* than do 6d or 7p. The 5f Coulomb energy $-Z^*e^2/\langle r\rangle$ is more negative ($\langle r\rangle$ is the expectation value of r,

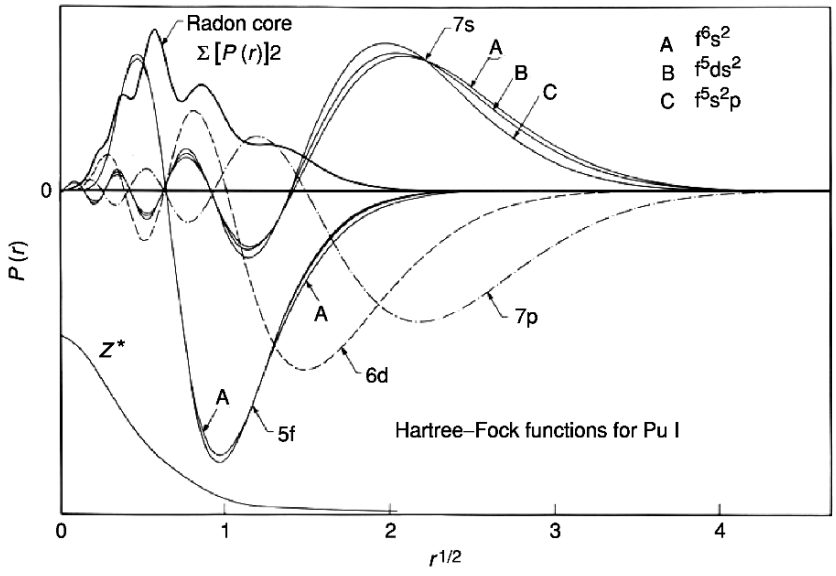

Fig. 16.5 *Radial distribution functions of valence electrons in neutral plutonium.*

i.e. r averaged over the radial density distribution). The total energy also includes a centrifugal term $+l(l+1)/r^2$ (l is the azimuthal quantum number), which tends to equalize the 5f, 6d, and 7p Coulomb energies, and the details vary along the actinide series as first shown by Goeppert Mayer (1941). It can be seen that the 7s radial function has its main contribution well outside the radon core, the 6d not quite so much, while the 5f electron is completely inside the core. The 5f electron is an inner electron and not much affected by the environment outside the core.

The determination of the electronic structure of the actinide elements through spectroscopy was expected to lend considerable knowledge to the chemistry of the elements. In fact the opposite is true because of complications in the observation and the analyses of the spectra, the chemistry was well known before elucidation of the spectra was possible. There are clear implications for actinide chemistry in the relative energies and radial distributions of the last ($Z-86$) electrons of a neutral actinide atom (see Fig. 16.5). For a typical actinide, the 6d and $7s^2$ electrons extend beyond the radon core and are available for forming chemical bonds, i.e. a typical actinide should be trivalent. At the beginning of the series, however, the 5f electron is not so firmly bound and has a larger $\langle r \rangle$, which reduces the amount of shielding of the nuclear charge as seen by the 6d electron. Hence for thorium, 6d is favored over 5f because of its larger Z^* and smaller centrifugal loss, and the ground state is $6d^27s^2$, resulting in a neutral atom with four external electrons (quadrivalent).

The tendency of the actinides to be multivalent in the first part of the actinide series because of the presence of 7s, 7p and 6d and 5f electrons of about equivalent energy is well known. The tendency to become more lanthanide-like in behavior toward the middle of the series and then have more divalent character near and beyond Es is related to the known electronic structure of these actinides. The increased stability of the 5f electrons as the atomic number is increased can be determined from the systematics of the electronic structure. At the heavy end of the actinide series, the 5f electrons become increasingly bound compared with 6d and it is more favorable to convert an added electron to another 5f, producing $5f^n7s^2$ as the ground state (divalent). This change in valence along the series is reduced in the lanthanides, as is shown in Fig. 16.6, where the relative energy of configurations $4f^n6s^2$, $4f^{n-1}5d6s^2$, and $4f^{n-1}5d6s6p$ are compared with the corresponding actinide configurations. The increased stability of 5f vs 4f in the second half of the series is evident and explains the tendency toward divalent character in the actinides beyond Es. The first actinide to show a stable divalent ion in solution was Md (Hulet *et al.*, 1967).

Brewer (1971a,b, 1984) developed methods based on the thermodynamic data of actinide metals and the regularities of the lowest energy levels of known actinide configurations (described above) to estimate the lowest energy levels of missing configurations of free atoms and ions in the 4f and 5f series.

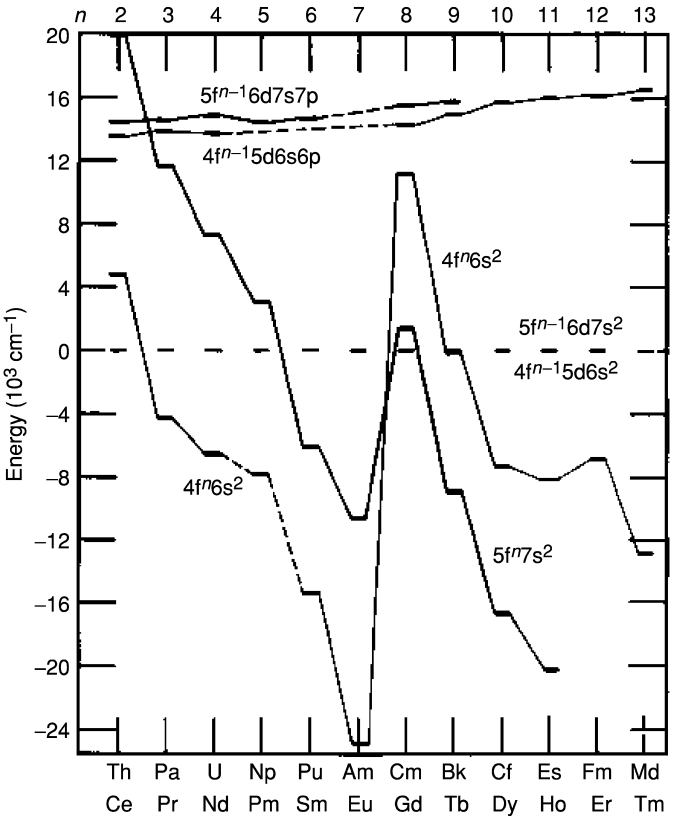

Fig. 16.6 *The energies of the lowest levels of the configurations, $f^n s^2$, $f^{n-1}ds^2$, and $f^{n-1}dsp$ for the actinides (5f) and lanthanides (4f) plotted vs n with the lowest level of the $f^{n-1}ds^2$ configuration at zero. Level energies with dashed level and connector lines are predicted values from Brewer* (1971a). *The lower energy for $5f^n7s^2$ for Cm and beyond is evident as the actinide series is ascended. This explains the tendency for the actinides to be more lanthanide-like at the center then become more divalent in character for the heavier actinides of Es and beyond.*

His estimates have proven to be very useful in assigning unknown configurations during spectral analyses.

These qualitative considerations are compared with some solution chemistry results in Fig. 16.7(a) and (b). The standard oxidation–reduction potentials $E^{\circ}(M^{(n+1)+}/M^{n+})$, converted from volts to cm^{-1}, are plotted for comparison with the energies of f–d transitions in free atoms. The full symbols are experimental values, the open symbols the calculated ones (Nugent, 1975). The similarity in shape of the two sets of curves is evident. There are approximate shifts of about 30000 cm^{-1} for the (III)/(II) potentials (Fig. 16.7(a)) and

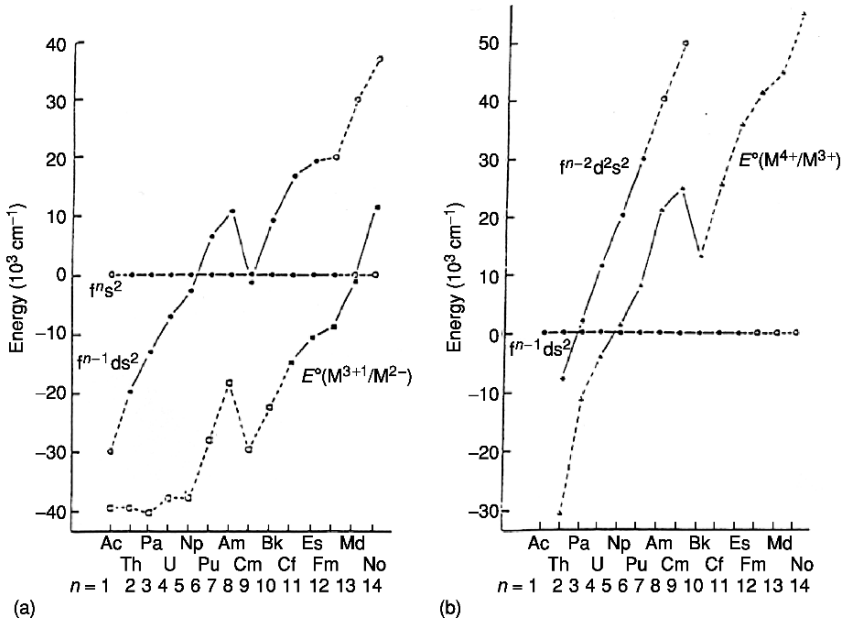

Fig. 16.7 *Comparison of actinide standard oxidation–reduction potentials and the relative energies of the series on converting a 5f electron to a 6d electron across the series.*

about 20000 cm^{-1} for (IV)/(III) (Fig. 16.7(b)) in the same direction, i.e. less energy is required for f→d conversion in solution than in the free neutral atom.

16.5 THEORETICAL TERM STRUCTURE OF THE FREE ACTINIDES

The energy of an atomic level results from various interactions and is an eigenvalue of the Hamiltonian operator describing the N-electron atom. If relativistic effects are first neglected, the Schrödinger equation $H\Psi = E\Psi$ is to be solved with

$$H = \sum_{i=1}^{N} \left(\frac{p_i^2}{2m} - \frac{Ze^2}{r_i} \right) + \sum_{i>j=1}^{N} \left(\frac{e^2}{r_{ij}} \right)$$

where $p_i^2/2m$ represents the kinetic energy and r_i the distance to the nucleus for electron i of mass m and electron charge e. The last term in H (named Q hereafter) accounts for the repulsions between all pairs of electrons separated by the distance r_{ij} and is too large to be treated as a perturbation. The central field approximation of Slater (1929), i.e. electrons being assumed to move in

a spherically symmetric potential $-U(r_i)/e$, gives the following equation H' considered as zeroth-order perturbation theory

$$H' = \sum_i \left(\frac{p_i^2}{2m} + U(r_i) \right).$$

The difference, H–H', is the perturbation potential,

$$H - H' = \sum_{i=1}^{N} \left(-U(r_i) - \frac{Ze^2}{r_i} \right) + \sum_{i)j=1}^{N} \left(\frac{e^2}{r_{ij}} \right)$$

The eigenvalues of H' depend on the n and l quantum numbers only, defining the configurations $\ldots n_a l_a^p n_b l_b^q \ldots$ and the first summation in the $H-H'$ equation contributes as a global shift for each configuration. The *active* two-electron part Q splits the highly degenerate states of the configurations into terms of definite total spin S and total orbital angular momenta L. Spin-dependent interactions have a leading term that couples the spin angular momentum s_i and the orbital angular momentum l_i of each of the electrons e_i. The spin–orbit operator

$$\Lambda = \sum_i \xi(r_i) s_i l_i$$

is then added to $H-H'$. The matrix elements of Λ have radial parts, the spin–orbit radial integrals ζ_{nl}, which increase rapidly with atomic number. Consequently, Λ can be considered a perturbation on SL terms for low Z elements only, where all levels with total angular momentum J ($\mathbf{J} = \mathbf{L} + \mathbf{S}$) allowed in a term ($| L - S | \leq J \leq L + S$) are close in energy. In actinides, the spin–orbit splitting (fine structure) of the terms is larger than their separations. LS coupling selection rules for transitions are violated and prevent total spin and orbital momenta S and L, respectively, from being quantum numbers of interest. The complexity of the actinide spectra is correlated with the relative magnitude of various parts in Q and in Λ. All the individual s and l angular momenta sum as $\mathbf{J} = \Sigma_i(\mathbf{s}_i + \mathbf{l}_i)$ with intermediate steps and the angular momenta associated with these steps define a coupling scheme. It is chosen so that the off-diagonal elements of the matrix of the $Q + \Lambda$ operator are as small as possible. In odd-Z elements, due to the nuclear magnetic moment $\mathbf{I}$ and its coupling with $\mathbf{J}$, the total angular momentum $\mathbf{J}$ should be replaced by $\mathbf{F} = \mathbf{I} + \mathbf{J}$. Then the hyperfine Hamiltonian $\mathbf{A} \cdot \mathbf{I} \cdot \mathbf{J}$ has to be added to $Q + \Lambda$. Actinides display the largest hfs patterns of all spectra; however, the hyperfine splitting is small compared with level separations and may be interpreted as a perturbation of the fine-structure levels with wave functions $|\alpha J M_J>$, α being a symbol for all couplings ending on J.

The angular and radial parts in the monoelectronic eigenfunctions and in the Hamiltonian operators lead to separate radial and angular integrals. All radial integrals needed in any configuration (electrostatic Slater integrals and spin–orbit integrals), and how they can be determined from experimental energy

levels in two-electron configurations, are fully described (Condon and Shortley, 1935). The application of this parametric approach to larger atomic systems needed Racah methods to be achieved. Racah derived the symmetry properties in configurations of l^N and the double tensor $\mathbf{w}^{(\kappa k)}$ properties of the operators involved in the Hamiltonian and showed how their ranks κ and k in the spin and orbital spaces explain selection rules and some singularities in matrix elements (Racah, 1942, 1943, 1949; Judd, 1963).

Although globally satisfactory, the first-order parametric theory faces certain problems. The electrostatic operator Q has matrix elements between configurations of the same parity $p = (-1)^{\Sigma l}$ and this would lead to the calculation of the H_1 operator with a basis set of many configurations. This was done with success by Racah (1950) for the two-electron configurations of Th III, but even with present-day computers the size of matrices that can be diagonalized is limited. Perturbation theory allows CI to be calculated as second-order effects, as long as they are distant (Rajnak and Wybourne, 1964). In case of f^n, two-particle operators lead to the correction terms $\alpha L(L+1) + \beta G(G2) + \gamma G(R7)$, where α, β and γ are effective parameters and $G(G2)$ and $G(R7)$ are Casimir operators of symmetry groups needed to classify f^n states. Three-particle operators involved in f^n to $f^{n\pm1}n'l'^{\mu l}$ excitations also lead to six additional parameters (Judd, 1966). In the case of several open shells, two-electron electrostatic operators lead to Slater-type effective parameters (Feneuille and Pelletier-Allard, 1968; Crosswhite, 1971). Although λ is an effective operator valid in a given configuration, second-order operators acting on spin and orbital spaces (cross products $Q \times \Lambda$) have been investigated (Goldschmidt, 1983). Further details are not given here as they can be found in several textbooks (Slater, 1960; Wybourne, 1965; Cowan, 1981; Rudzikas, 1997).

Judd (1985) has made a survey of atomic structure theory for complex spectra. He included a new way of parameterization. Radial integrals and the usual effective parameters are correlated in the sense that the introduction of a neglected parameter changes the values of those already used in the analysis. This can be overcome by replacing the usual operators by linear combinations associated with 'orthogonal' parameters. An application to Pr III $4f^3$ was made (Judd and Crosswhite, 1984) and the angular coefficients of relevant operators were further studied (Hansen *et al.*, 1996; Judd and Lo, 1996) but the actinides have not yet been investigated in this way.

16.6 DETERMINATION OF RADIAL PARAMETERS

A description of the level structure of an actinide configuration as given by the eigenvalues and eigenvectors of the energy matrix H has been outlined above. To obtain quantitative information, it is necessary to provide numerical values for the matrix elements and then to diagonalize the matrix. The problem thus divides naturally into several stages: evaluating the angular coefficients f_k, g_k of

the electrostatic integrals $R^k(n^a l^a\, n^b l^b, n^c l^c\, n^d l^d)$ with ($a = c$, $b = d$) for the direct Slater integrals, F^k, and ($a = d$, $b = c$) for the Slater exchange integrals, G^k. The same procedure may be applied for the spin–orbit integrals, for the electrostatic CI integrals R^k, and for effective CI parameters. Then initial values are provided for the radial integrals and the effective parameters, followed by diagonalization and optimization of the effective parameters by comparison of the calculated energy levels with the assigned experimental levels.

The angular coefficients are calculated exactly by application of the Wigner–Eckart theorem and by means of Racah algebra techniques as described by Judd (1963). They are products of phase factors, n–j symbols, and contain sums over the states of the parent configuration f^{n-1} as the decoupling of one (or more) f electrons out of f^n is needed. For that purpose, fractional parentage coefficients can be found in Nielson and Koster (1964). The analytic expression of angular coefficients was used as input in the first computer programs to determine numerical values of the angular coefficients (Racah, 1951; Bordarier, 1970). As an intricate function of all spin and orbital momenta involved in the selected coupling scheme, it was subject to errors although an implicit check of the Racah algebra consistency was provided by the integer form $a(b)^{1/2}/c$ of the whole numerical process. A nearly automatic code was developed at LANL (Cowan, 1968, 1981), requiring only the number of electrons in each open shell, input of the fractional parentage coefficients, and a list of terms for each shell. This code is widely distributed and was adapted at other sites, such as ANL (Crosswhite, 1975) and for PC users (Kramida, 1997). It runs faster than the earlier codes as all calculations are performed in the decimal form.

After an initial set of radial integrals is chosen, the Slater–Condon method of treating them as adjustable parameters may be applied. Upon diagonalization, the eigenfunctions lead to coefficients of the parameters in intermediate coupling and to a linear expansion for the energy of each level. In the subsequent least-squares minimization of $\Delta_i = E_i(\text{exp})$–$E_i(\text{th})$ (where $E_i(\text{exp})$ and $E_i(\text{th})$ are the experimental and calculated levels), and the mean error $\sigma = (\Sigma \Delta_i^2/(N_{\text{lev}}$–$N_{\text{par}}))^{1/2}$ measures the quality of the fit and is critically dependant on the number of known levels N_{lev} relative to the number N_{par} of unknown parameters. Some iterations of the diagonalization/least-squares fits lead after convergence to a set of fitted parameters with standard errors. In the complex first and second spectra, inappropriate initial parameters may lead to term inversions in the comparisons of $E_i(\text{exp})$ vs $E_i(\text{th})$ and it sometimes happens that iterations diverge when processed in an automatic way.

Besides obtaining a low mean error on energies, validity checks of the parametric study may be obtained by using the eigenfunctions for the calculations of hfs constants. This was done for U I (Avril *et al.*, 1994). In addition, theoretical studies of the IS may be used, e.g. in Th(I,II) (Blaise *et al.*, 1988a). For even-Z elements, all investigated with the support of Zeeman effect, first checks are provided by comparisons between large sets of Landé factors $g_i(\text{exp})$ and easily derived $g_i(\text{calc})$ values.

16.7 ACTINIDE PARAMETERS

16.7.1 Least-squares fitted values

Actinide parameter values cannot be derived in a straightforward way because of the difficulties discussed above. In almost no case can the parameters be determined precisely; the values obtained depend on the assumptions made in defining the energy matrix and these vary from case to case and cannot be compared reliably. The early actinides (Th to Np) are more completely known but have more close configurations, and so the parameter values derived are sensitive to how much CI is included. The middle actinides (Pu to Cf) have larger configuration separations but more terms in each, leaving the choice between complete configurations with CI neglected or truncated subconfigurations with CI considered. The late actinides (Es and beyond), which get some simplicity being closer to $5f^{14}$, may provide values that are still unavailable from lower-Z elements. A rare example taken from einsteinium (Worden *et al.*, 1974; Blaise *et al.*, 2003) is shown in Fig. 16.8. In the first excited configuration of Es I $5f^{11}7s7p$, the lowest level $^4I_{15/2}$ of the core $5f^{11}$ is relatively well isolated from others and the relationships $Q(7s,7p) > \Lambda(7p) > Q(5f,7s)$, $Q(5f,7p)$ lead to a case

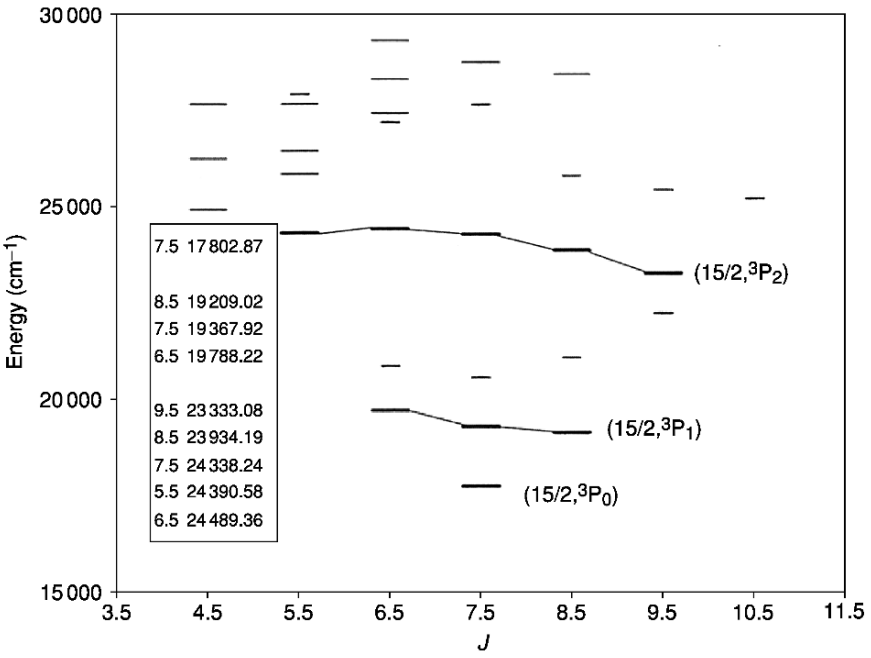

Fig. 16.8 *The low-lying levels for various configurations of Es I. The experimental values for the $5f^{11}7s7p$ of Es (heavy bars) are grouped in J_c–J_2 multiplets. Some predicted levels of $5f^{10}6d7s^2$ (light short bars) and of $5f^{11}7s7p$ (light long bars) are also given.*

of ($5f^{11}$ J_c–($7s7p)^3P$ J_2) J coupling with a clear separation of (15/2, $^3P_0$) and multiplets (15/2, $^3P_1$) and (15/2,$^3P_2$). As the theoretical splitting of any sp^3P term is approximately equal to $1.5\zeta_p$, an approximate value of 4100 cm^{-1} is readily derived for the ζ_{7p} spin–orbit parameter. Conversely, a case of complexity characterizing most of the lanthanides is found in the study of $5f^36d7s^2$ + $5f^36d^27s$ configurations of U I (Petit, 1999) using an extended version of RCG/RCE codes (Cowan, 1981). The complete basis sets of both configurations lead to 3642 theoretical levels, of which 155 are identified and 29 parameters are fitted with an excellent mean error. The eigenfunctions of the lower levels describe Landé g-values properly. On the other hand, the lack of experimental evidence for the expected perturbing configuration $5f^36d^3$ and the large number of levels without g-values or IS set the limit for additional theoretical assignments.

The small value of the ratio $N_{known}/N_{predict}$ mentioned for U I is usual in the I (free atom) and II (singly ionized ion) spectra of f-elements. Not all parameters involved in the description of a configuration can be derived reliably from the least-squares fitting on its very low energy part. If SL coupling is obeyed, all levels of a term have the same dependence on Slater integrals and the determination of the F^k(ff) ($k = 0,2,4,6$) parameters would require at least four terms of f^n to be known, which is not fulfilled in many free atoms and ions of actinides. The lowest terms of highest multiplicity have separations that are a function of only one parameter, the Racah parameter $E^3 = (1/135)F^2 + (2/1089)F^4 - (175/42471)F^6$. Owing to the strength of the 5f spin–orbit interaction, its off-diagonal matrix elements lead to term mixings and those intermediate coupling conditions lead to the differentiation of the coefficients of the electrostatic parameters for all the levels. Hence the least-squares fit does yield values of all the F^k(ff) but with rather large statistical errors.

In order to reduce those statistical errors and to improve the predictive character of the parametric calculations, the techniques of generalized least-squares (GLS) first used by Racah and coworkers in 3d-elements have been applied to actinides (Blaise *et al.*, 1980). It is known that for long periodic trends, the parameters determined as described above have a slow empirical dependence on Z. The simple expansions of the parameters as $P = A(P) + (n–7)B(P) + (n–7)^2C(P)$ lead to the determination from all the known levels of $5f^n7s^2$ and $5f^n7s$, of the A, B, and C GLS-constants for the parameters F^k(ff), α, β and γ. In the singly ionized free ion spectra, 112 levels of seven elements from U II $5f^47s$ through Es II $5f^{11}7s$ were interpreted by this GLS method with 22 free parameters and a small error of $\sigma = 84$ cm^{-1}.

16.7.2. Comparisons with *ab initio* radial integrals

Various *ab initio* studies of atomic systems have confirmed Racah's empirical statement that in $3d^n$ atoms and ions the radial integrals are smoothly Z-dependent. The same trends are found in the 4d, 4f, 5d, and 5f elements. Consider the theoretical values from relativistic HF (HFR) calculations

(Crosswhite, 1975). Fig. 16.9(a) shows various cases with certain regularities. The integrals F^k(ff) all increase with atomic number, the increase approaching linearity for the second half of the series. The ratios of the limiting slopes of F^2:F^4:F^6 are 1:0.643:0.464. The numerical values of the integrals for $5f^n7s^2$ are for Th I 49704:31366:22660 = 1.0:0.631:0.456 and for Fm I 90499:58914:43210 = 1:0.651:0.477. For hydrogenic-shaped 5f radial functions, the ratios are 1:0.688:0.527. The similarity to hydrogen can be taken to mean that over the range in r which includes most of the HF 5f radial function, the potential does not change greatly from that for a fairly constant effective nuclear charge Z^*. The increase of the F^k integrals with Z corresponds to the actinide contraction.

Fig 16.9(a) shows that the HF values of F^k(ff) are only mildly affected by changes in the outer electrons and for each k, converge toward the same limit with increasing Z, independent also of ionic charge. The change in the integral for constant Z but varying number of 5f electrons is much greater and amounts to a constant shift. All these effects are in the direction expected for changes in the shielding of the 5f electrons. The HFR overlap integrals F^k(5f6d) and G^k(5f6d) in Fig. 16.9(b) and (c) show the opposite effect: they decrease with Z because the 5f functions contract while the 6d functions remain constant, and they are more sensitive to the number of 7s electrons, that affects their relative shielding. The one-electron integrals ζ_f, which are proportional to $<1/r^3>$, increase with Z and their dependence on outer electrons is consistent with shielding effects. The effect of increasing Z on ζ_d and ζ_f is shown in Fig. 16.9(d).

Now consider the experimental parameters and how they compare with theory. Table 16.3 presents some experimental values of F^k(ff) parameters, the corresponding HFR integrals and several ways of comparing them. The experimental parameters P_{exp} are all smaller than the calculated integrals P_{HFR}, which is an almost universal characteristic throughout the periodic table. The ratio (P_{exp}/P_{HFR}) is roughly 2/3 with irregular variations. Another ratio is F^k/F^2 that can be formed independently for P_{exp} and P_{HFR}. A third possibility is the difference (P_{exp}–P_{HFR}) that was found to be nearly constant for each F^k for tripositive lanthanide ions (Carnall *et al.*, 1978). It should be stressed that parameter comparisons are meaningful only if they have been derived with similar approximations, i.e. the same terms in the Hamiltonian operator were calculated on similar sets of configurations, only the number n of core electrons being varied. Parametric studies still continue to make general trends better known.

16.8 SUMMARY OF ACTINIDE CONFIGURATIONS

Table 16.1 lists the lowest level of all known actinide configurations of the species studied and Table 16.2 shows the lowest level of some common configurations of the neutral actinide spectra. Thousands of higher levels are known, but for this survey we are more interested in generalities than in details. The

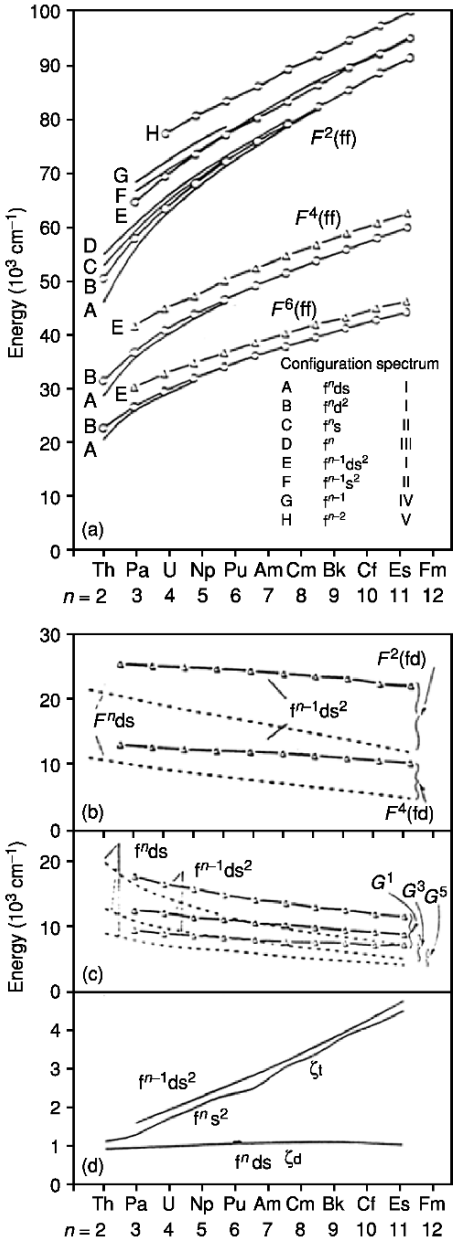

Fig. 16.9 *Relativistic Hartree–Fock calculations of some actinide radial integrals:* (*a*) $F^k(ff)$; (*b*) $F^k(fd)$; (*c*) $G^k(fd)$, *and* (*d*) ζ_f *and* ζ_d.

Table 16.3 *Some experimental values of F^k(ff) parameters, Hartree–Fock values, and ratios F^k/F^2 for a number of actinide elements.*

					F^k/F^2				
Configuration	*Element*	*Parameter*	*Experiment*	*Hartree–Fock*	*Expt*	*HF*	F^k_{Expt}/F^k_{HF}	$F^k_{HF} - F^k_{Expt}$	*References*
$5f^4 7s^2$	U(I)	F^2	36 505	62 891	1.000	1.000	0.580	26 386	Rajnak (1979)
		F^4	28 474	40 290	0.780	0.641	0.707	11 816	
		F^6	20 808	29 304	0.570	0.466	0.710	8496	
$5f^5 7s^2$	Np(I)	F^2	39 797	67 452	1.000	1.000	0.590	27 655	Crosswhite (1986)
		F^4	31 017	43 381	0.779	0.643	0.715	12 364	
		F^6	23 044	31 611	0.579	0.469	0.729	8567	
$5f^6 7s^2$	Pu(I)	F^2	42 935	71 461	1.000	1.000	0.601	28 526	Crosswhite (1986)
		F^4	33 472	46 094	0.780	0.645	0.726	12 622	
		F^6	24 959	33 638	0.580	0.471	0.742	8679	
$5f^8 7s^2$	Cm(I)	F^2	51 025	78 531	1.000	1.000	0.650	27 506	Crosswhite (1986)
		F^4	39 133	50 868	0.767	0.648	0.769	13 883	
		F^6	30 579	37 204	0.599	0.474	0.822	8229	
$5f^{10} 7s^2$	Cf(I)	F^2	57 870	84 799	1.000	1.000	0.682	26 929	Wyart (1998)
		F^4	45 052	55 085	0.779	0.650	0.818	10 033	
		F^6	31 873	40 345	0.551	0.476	0.790	8472	
$5f^3 6d7s^2$	U(I)	F^2	43 891	68 684	1.000	1.000	0.639	24 793	Petit (1999)
		F^4	32 431	44 396	0.739	0.646	0.730	11 965	
		F^6	23 128	32 417	0.527	0.472	0.713	9289	
$5f^4 6d7s^2$	Np(I)	F^2	43 317	72 662	1.000	1.000	0.596	29 345	Crosswhite (1986)
		F^4	37 170	47 094	0.858	0.648	0.789	9924	
		F^6	23 286	34 436	0.538	0.474	0.676	11 150	
$5f^5 6d7s^2$	Pu(I)	F^2	47 975	76 279	1.000	1.000	0.629	28 304	Wyart (1998)
		F^4	37 590	49 543	0.783	0.649	0.758	11 953	
		F^6	33 441	36 268	0.697	0.475	0.921	2827	

trend of analogous configurations as a function of atomic number in the neutral atoms has been shown in Figs. 16.3(a), (b), and 16.6. The relative configuration energies as a function of ionization stage are given in Table 16.4 for Th I–IV 5f, 6d, 7s, and 7p, showing that the 5f configuration becomes increasingly more stable as outer electrons are removed (5f gains 17000 cm^{-1} over 6d in going from Th I to Th IV). The change in 5f energy with increase in atomic number corresponds to the actinide contraction, which increases the effective nuclear charge Z^*. Increasing ionization also increases Z^* by reducing the shielding of 5f electrons from the nucleus as outer electrons are removed. The effect on the 5f energy is thus in the same direction as with increasing Z. The outer electrons 7s and 7p are more nearly hydrogenic and have energies that become more negative as approximately the square of the ionic charge (about the same for all Z). Hence the 7s–7p difference increases with ionic charge.

Racah (1950) treated the term structure of Th III in a classic paper on least-squares parameter fitting in intermediate coupling with CI. With these off-diagonal matrix elements included, the calculated energies were in much better agreement with observation, and in addition, the calculated g-values were also in better agreement than the pure SL Landé g-factors. This has been the general experience in fitting spectra with more than two electrons: the better the energy fit, the better the g-value fit; it also applies to other properties such as IS, hfs, and relative intensities of transitions, and thus lends confidence to the calculation. Attempts to make the g-value fit more exact by trying to fit the energies and g-values simultaneously have not been successful because these are not independent quantities. If the calculated g-values are not more or less in agreement with observation, it is an indication that some interactions are missing from the energy matrix. Since parameter fits in the general case are not exact and are in a state of flux, no attempt has been made in Table 16.1 or 16.2 to try to include calculated g-values or other calculated properties. Comparison of g (exp) with calculated SL g-values serves as an indication of how much intermediate coupling and CI are present and not that the assignment is in doubt. Tables 16.1 and 16.2 show that, in moving toward the middle of the actinide series, the multiplicity increases in accord with Hund's rules.

Thus in Pa I (the first true actinide with a 5f electron in the ground state), there are quartets and sextets (and also doublets in the higher states), whereas in Am I there are octets and decets (and also sextets, quartets, and doublets). This has a profound effect on the intensity distribution of the observed spectral lines. In pure SL coupling, there is a selection rule $\Delta S = 0$ (octet terms have transitions only to octets, etc.). In intermediate coupling, as obtains in the actinides, there are off-diagonal spin–orbit matrix elements between terms of adjacent multiplicity ($\Delta S = 0, \pm 1$), which means that octet terms, for example, will also have some decet and sextet eigenvector components, and therefore have transitions to decet and sextet terms. There will be, however, no transitions to quartet and doublet terms. The strong lines (those involving the low terms) will therefore consist of transitions between terms of high multiplicity that are

Table 16.4 *Comparison of thorium configurations in four stages of ionization.*

Th IV (Th^{3+})		*Th* III (Th^{2+})		*Th* II (Th^{+})		*Th* I (Th^{0})	
Configuration	*Level* (cm^{-1})	*Configuration*	*Level* (cm^{-1})	*Configuration*	*Level* (cm^{-1})	*Configuration*	*Level* (cm^{-1})
5f	0	5f 7s	2527	$5f\,7s^2$	4490	$5f\,7s^27p$	18 432
6d	9193	6d7s	5524	$6d7s^2$	1860	$6d7s^27p$	10 783
Δ(5f–6d)	–9193		–2997		2630		7649
7s	23 130	$7s^2$	11 961	$6d7s^2$	4113	$6d^27s^2$	0
7p	60 239	7s7p	42 260	6d7s7p	23 373	$6d^27s7p$	14 465
Δ(7s–7p)	–37 109		–30 299		–19 260		–14 465

comparatively few in number. There will also be transitions among the terms of low multiplicity but these will be very numerous and weak. The observed Am I spectrum thus consists of a relatively small number of strong lines superimposed on a weak complex background. The strong lines are easy to classify into a transition array; the weak lines are not. The determination of the G^k parameters requires knowledge of terms of all multiplicities, not obtainable from just the strong lines. At the beginning of the actinide series, by contrast, the multiplicities are all low and the ΔS selection rule is not so restrictive, hence the range in intensity is not so great. In fact Pa I appears at first sight to have the most complex spectrum of all the actinides because of the comparatively uniform intensities, despite fewer expected terms. The Pa spectrum is further complicated by the presence of hfs. Many transitions have four hfs components that have a large degradation in intensity because of the low nuclear spin (^{231}Pa, $I = 3/2$) and low J values, so they often cannot be distinguished from neighboring weak lines. In Am (for the relatively long half-life isotopes ^{241}Am and ^{243}Am, $I = 5/2$), each level has six hfs components when $J \geq 5/2$, in Bk and Es (for ^{249}Bk and ^{253}Es, $I = 7/2$) each level has eight hfs components when $J \geq 7/2$, with less degradation so they usually stand out from the background. Hence the analysis and interpretation of a spectrum like Pa is no easier than for later elements with larger multiplicities.

Another characteristic of the actinide series is the fact that the L values for f^n go through a maximum not at the half-filled shell, as in the case of the S values, but at the one-fourth and three-fourths-filled shells. Thus the ground state of Np I f^4ds^2 is $^6L_{11/2-21/2}$ and for Np(I) f^4d^2s it is $^8M_{11/2-25/2}$. These high J values are poorly excited by electron collision in the light source, so transitions to the highest J levels are weak and hard to find, in contrast to multiplets at the beginning of the actinides. For the three-fourths-filled f^n shell, the multiplets are inverted and not so much of a problem. The high L values for Np have a considerable effect on the hfs because the large orbital angular momentum produces a high magnetic field at the nucleus that increases the orbital contribution. The Np I ground level has a total width of 0.776 cm^{-1} in spite of having no unpaired s-electron, the usual source of large hfs (Fred *et al.*, 1977). Bk I and Es I have even larger widths, 1.150 and 1.532 cm^{-1}, due to larger nuclear spin, larger J value, and larger Z (Worden *et al.*, 1974, 1987). The ability to measure the intervals of the hfs patterns to better than 1 part in 1000 is a great help in the empirical analysis of these spectra. Moreover, the quantum numbers of the various levels can be obtained by comparing the relative widths with those calculated by standard hfs theory.

To summarize, the spectroscopic properties of all the actinide elements that can be studied by conventional emission spectroscopy, Ac to Es, have now been investigated experimentally and theoretically. The present status is satisfactory in that most of the electronic structure information of interest for actinide chemistry is available. The experimental completion of the determination of the electronic structure of the last four elements in the actinide series will

take considerable effort and new techniques due to the limited availability of the elements and their short half-lives. Theoretical estimates together with extrapolations (e.g. Vander Sluis and Nugent, 1972; Brewer, 1984) from the known structure of the lower actinide elements are needed. In addition, further efforts are required to provide the complete details for some of the lighter actinide elements.

16.9 NEW PROPERTIES OF ACTINIDES DETERMINED BY CONVENTIONAL SPECTROSCOPY AND MATERIAL LEFT FOR DATA REDUCTION

The signs of the nuclear magnetic moments in both ^{249}Cf and ^{251}Cf have been determined to be negative (Conway *et al.*, 1995). From the examination of the direction of degradation of the hfs of the ground and first excited levels in the second spectrum of ^{249}Cf, the $^{6}I_{17/2}$ and the $^{4}I_{15/2}$ of $5f^{10}7s$ were found to be inverted and regular, respectively. Since the hfs of both isotopes degraded in the same direction, it was concluded from this data that the sign of the nuclear magnetic dipole moment of both isotopes is negative. The nuclear spins of both isotopes were confirmed as 9/2 for ^{249}Cf and 1/2 for ^{251}Cf. A large number of ^{251}Cf lines with two components were observed indicating the nuclear spin of this isotope is 1/2. With the high J values involved in most Cf transitions, the off-diagonal components for ^{251}Cf are very weak (3% or less of the total intensity when $J > 3$) (White, 1934) and so they were not observed in the spectra resulting in many lines with two components.

There is considerable actinide spectroscopic data awaiting analyses. One complete set of photographic plates for Bk taken on the ANL spectrograph is in storage at LLNL. The Bk structure was determined from measurements of photographic plates taken on a 3.4 m Ebert spectrometer with a special high-angle grating and order sorter (the resolution and dispersion were about equal to that of the ANL spectrograph). Worden, using a Grant comparator at LLNL, measured the plates and then the data were analyzed (Worden *et al.*, 1987). Some of the Zeeman spectra taken on the ANL spectrograph were measured (again by Worden) to determine Landé g-values used in the level analyses. A complete set of plates was taken in 1976 on the ANL spectrograph using EDLs with the major isotope ^{250}Cf and known ^{249}Cf, ^{251}Cf, and ^{252}Cf content, including some with an additional spike of ^{252}Cf. The IS values for ^{250}Cf vs ^{249}Cf, ^{251}Cf, and ^{252}Cf should result from measurements of these plates as well as a better set of wavelengths (there are no hfs and subsequent broadening with ^{250}Cf as there is with the current ^{249}Cf-line list). Improved analyses of the neutral and especially the first ion spectra (where the hfs is larger) should be possible.

The complete Es spectrum was measured on the ANL spectrograph in 1975. Earlier measurements were done at LLNL (Worden *et al.*, 1974). The ANL

photographic plates should produce a much more complete list and many more levels should be obtained. Blaise and Wyart are currently working on these data to improve the analyses of the Es I and II spectra (Blaise *et al.*, 2003; Wyart *et al.*, 2005).

16.10 LASER SPECTROSCOPY OF ACTINIDES

A large number of hfs A and B factors for ^{235}U have been determined by laser spectroscopy. The data list included 35 odd (28 low-lying odd levels of the configuration $5f^36d7s^2$) and 34 even levels from 15500 to 31000 cm^{-1}, many with very high precision (Childs *et al.*, 1979a,b; Hackel *et al.*, 1979; Greenland *et al.*, 1981; Avril *et al.*, 1986, 1994; Demers *et al.*, 1986). A very large number of high-lying upper levels of both parities have been found by multi-step laser spectroscopy of U by researchers in the USA, France, England, India, Japan, and China. However, these level determinations are inaccurate (uncertainties ranging from 0.5 to 2 cm^{-1}) as compared with typical emission spectra levels derived from grating spectrographs or FTS instruments (with 0.02 to 0.001 cm^{-1} uncertainty) so no references are given.

The signs of the ground state A and B factors of neutral ^{241}Am (Le Garrec and Petit, 1986) and ^{243}Am (Meisel *et al.*, 1987) have been determined by high-resolution laser spectroscopy of the Am isotopes to be $A < 0$ and $B > 0$. The ^{242m}Am isotope has the same sign because the hfs has the same degradation. Considerable laser spectroscopy of Pu has been accomplished, but little except the IP has been published in the open literature (Worden *et al.*, 1993). The same is true of Np where the energy separation of 24.27 cm^{-1} between the two lowest levels of Np II (Fred and Blaise, 1978) was used to help confirm the observation of Rydberg series in Np I (Worden and Conway, 1979). A review of multi-step laser excitation of lanthanides and actinides has been published (Worden and Conway, 1980) with a discussion of properties that can be determined by the use of laser spectroscopy.

16.11 IONIZATION POTENTIALS OF ACTINIDES BY LASER SPECTROSCOPY

The precise determination of the first IP of the actinide elements is important for the identification of systematic trends in binding energies of the elements. It is also important for drawing conclusions about the electronic structure of the atoms, since the first IP is directly connected to the atomic spectra. Information about the electronic structure of the actinides is required to predict deviations from the regularities of the periodic table (Pyykkö and Desclaux, 1979) caused by relativistic effects which are expected in this region as a result of the relativistic mass increase of the inner electrons (Pyykkö, 1988). The IPs are useful

quantities in the Born–Haber cycle (Morss, 1971) and also allow comparison with predictions of multi-configuration Dirac–Fock calculations (Fricke *et al.*, 1993), a successful theoretical treatment for heavy multi-electron atoms.

Ionization energies of the neutral atoms were derived by Sugar using interpolation of the series properties of the $5f^n7s8s$ configurations. They are given in Table 16.5 (Sugar, 1974). The first accurate experimental value of an IP of an actinide element was by multi-step laser spectroscopic observation of reasonably long high-energy Rydberg series in uranium by Solarz *et al.* (1976) who obtained the value 49958.1(4.0) cm^{-1}. In the Solarz technique, delayed ionization by use of a CO_2 laser was employed to separate the short-lived valence levels from the long-lived Rydberg levels enabling their detection in the very complex spectrum. The photoionization limit was often determined first to limit the scan range needed for measuring Rydberg levels to less than 50 to 100 cm^{-1}. Such a limit is usually easy to detect by the sharp rise in ions as the photoionization laser is scanned in a multi-step excitation scheme. These were normally determined with the apparatus used in the configuration without delayed field ionization (Worden *et al.*, 1978). In an experiment similar to that of Solarz *et al.*, Coste *et al.* (1982) used delayed field ionization to measure an

Table 16.5 *First IPs (IP_{exp}) of the actinide elements determined by RIMS. Tabulated are also IPs (IP) from laser spectroscopy measurements. The method and reference is given in column* 5 *(RA = comparison of lifetimes of Rydberg and autoionizing states, RC = Rydberg convergence limits). The predictions by extrapolation of spectroscopic data* (*Sugar*, 1974) *are given in column* 6.

Actinide element	$IP_{exp.}$ (cm^{-1}) (*RIMS*)	$IP_{exp.}$ (eV) (*RIMS*)	*IP* (cm^{-1}) (*others*)	*Method and references*	*Extrapolated* (*Sugar*, 1974)
Ac	43 398(3)	5.3807(3)			41 700(1000)
Th	50 867(2)	6.3067(2)	50 890 (20)	RA (Johnson *et al.*, 1992)	49 000(1000)
Pa	—	—			47 500(1000)
U	49 957(2)	6.1939(2)	49 958(4)	RC (Solarz *et al.*, 1976)	48 800(600)
			49 958.4 (5)	(Coste *et al.*, 1982)	
Np	50 535(2)	6.2655(2)	50 536(4)	RC (Worden and Conway, 1979)	49 900(1000)
Pu	48 601(2)	6.0258(2)	48 604(1)	RC (Worden *et al.*, 1993)	48 890(200)
Am	48 180(3)	5.9736(3)			48 340(80)
Cm	48 324(2)	5.9914(2)			48 560(200)
Bk	49 989(2)	6.1978(2)			50 240(200)
Cf	50 665(2)	6.2817(2)			50 800(200)
Es	51 358(3)	6.3676(3)			51 800(200)

RA, Rydberg autoionization; RC, Rydberg convergence of relative long series.

IP of 49958.4(5) cm^{-1} for the U atom. The IP of neutral Np was measured at 50 536(4) cm^{-1} using similar laser techniques (Worden and Conway, 1979). These values are, respectively, 2 and 1% larger than Sugar's estimates (see Table 16.5). Rydberg levels have been measured by delayed field ionization and were created by a number of different processes (Worden *et al.*, 1978; Worden and Conway, 1980) including collisional ioniziation converging to the ground state and auto-ionization levels converging to excited levels in the ion. The IP of ^{239}Pu was measured using a number of laser methods by Worden *et al.* (1993) to obtain the value 48 604(1) cm^{-1}. The experiments included the observation and measurement of hfs of ^{239}Pu and the IS of ^{240}Pu–^{239}Pu in auto-ionization levels, the first such measurement for an actinide.

16.12 FIRST IONIZATION POTENTIALS OF THE ACTINIDES BY RESONANCE IONIZATION MASS SPECTROMETRY

The first IPs of the common lighter actinide elements Th, U, Np, and Pu have been determined by laser spectroscopy (Solarz *et al.*, 1976; Worden and Conway, 1979; Coste *et al.*, 1982, Johnson *et al.*, 1992; Worden *et al.*, 1993). The most precise measurements were performed by the study of long-lived Rydberg series converging to one or more limits in the ion. For these elements, gram amounts of the metal were readily available for use in experiments. About 1 g of material was used to determine the IP of Np by these techniques (Worden and Conway, 1979). As much as 2 g of ^{239}Pu was used for the determination of the IP of ^{239}Pu by the observation of the threshold of ionization and of a large number of Rydberg series that converged to five separate limits in the ion (Worden *et al.*, 1993). A large amount of other types of spectroscopy was done with these samples that was not part of the IP determination and has not been published.

RIMS, first developed for ultra-trace analysis of actinide nuclides (Ruster *et al.*, 1989), has been introduced as a method that allows the accurate determination of the first IP of the actinides with samples of only 10^{12} atoms ($\sim$400 pg) or less. This makes possible the measurement of IPs of the heavier actinides and some light actinides that can be conveniently handled only in small quantities because of the strong radioactivity or that may be available only in very limited amounts.

The method is based on the determination of the photoionization thresholds in the presence of an external electric field and is explained in detail in a number of papers (Riegel *et al.*, 1993; Trautmann, 1994; Köhler *et al.*, 1997; Erdmann *et al.*, 1998). There it is shown that the observed ionization threshold is proportional to the square root of the electric field strength E. For the determination of the first IP, the wavelength of the laser for the ionizing step in a multi-step process is scanned across the threshold in the presence of E. The ionization threshold $W_{th}(E)$, the total energy of the exciting lasers, is indicated by a sudden increase of the ion count rate. This procedure is repeated for various electric

field strengths and the extrapolation of $W_{th}(E)$ to zero field strength leads to the energy of the first IP.

The experimental set-up (Ruster *et al.*, 1989) for resonance ionization mass spectrometry generally consists of three tunable dye lasers pumped by two pulsed copper vapor lasers (6.5 kHz pulse repetition rate, with 30 and 50 W average output power, 30 ns pulse duration) and a time-of-flight (TOF) mass spectrometer. The dye laser beams are focused into the TOF region where they interact perpendicularly with the atomic beam of the element under investigation. Ionization by two- or three-step resonant laser excitation takes places in the presence of an electric field. The importance of 6.5 kHz excitation is for efficient excitation of the atoms in the atomic beam of this set-up. Special care is taken to make the electric field homogenous and to keep it free of stray electric fields by use of corrective electrodes.

For the determination of the first IP of actinium (Waldek *et al.*, 2001), a frequency doubled titanium–sapphire laser pumped by a NdYAG laser (Grüning *et al.*, 2004) was used for one-step resonant excitation and a dye laser for the ionization step. In all experiments, the wavelengths of the laser beams were measured by pulsed wavemeters with a precision of $\Delta\lambda/\lambda = 10^{-6}$.

One crucial part for the application of resonance ionization mass spectrometry to determine the first IP is the creation of an atomic actinide beam. This is achieved by resistive heating of a sandwich filament consisting of a thin tantalum foil on which the element under investigation is electrochemically deposited in the form of the hydroxide (3 mm spot) and covered with a thin layer ($\sim$1 μm) of titanium or zirconium produced by sputtering. By heating such a sandwich filament, the hydroxide is converted to the oxide, which is reduced to the metallic state during diffusion through the covering layer. For the elements of uranium up to fermium, a titanium layer was used whereas for actinium the reduction by titanium was not efficient and therefore zirconium was used. Efficient release from these filaments occurs at temperatures between 800 and 1200°C, depending on the element. For protactinium, it was not possible to produce an atomic beam in this way, not even with thorium as reducing agent. As a result, an experimental value of the first IP of protactinium with RIMS is still missing.

For all the measurements of the photoionization thresholds either two-step (Ac, Np) or three-step (Th, U, Pu, Am, Cm Bk, Cf, Es) excitation schemes were used, each starting from the atomic ground state (Table 16.6). The wavelengths for the excitation steps were selected by use of energy levels published by Blaise and Wyart (1992) or by finding levels with scans of the appropriate laser. The photo-ionization thresholds were determined with various electric field strengths of 1.6–340 V cm^{-1}. The precision of the photo-ionization threshold method was checked by the re-determination of the first IP of Th, U, Np, and Pu. There is excellent agreement as can be seen from Table 16.5. With quantities of only $\sim 10^{12}$ atoms each, the first IPs of Ac, Am, Cm, Bk, Cf, and Es were determined for the first time by RIMS. Plots of the obtained ionization

Table 16.6 *Excitation schemes of the actinide elements used for the determination of the first IP by RIMS. The last step laser wavelength is approximate because the laser is scanned in the presence of an electric field of various voltages.*

Actinide element	λ_1 (nm) *air*	*First excited state* (cm^{-1})	λ_2 (nm) *air*	*Second excited state* (cm^{-1})	*Ionizing* λ (nm)
Ac	388.56	25 729.0	—	—	≈568
Th	580.42	17 224.3	622.90	33 273.8	≈568
U	639.54	15 631.9	591.47	32 534.1	≈577
			585.85	32 696.3	≈582
Np	311.81	32 061.3	—	—	≈541
Pu	648.89	15 406.6	629.57	31 285.9	≈579
Am	640.52	15 608.5	654.41	30 885.1	≈578
Cm	655.46	15 252.2	640.56	30 859.1	≈573
Bk	565.90	17 666.0	720.50	31 541.3	≈544
			664.52	32 710.3	≈581
Cf	572.61	17 459.2	625.04	33 453.7	≈583
Es	561.53	17 803.5	661.13	32 924.9	≈544

thresholds of these elements versus the square root of the applied electric field strength E are shown in Fig. 16.10. The values fit perfectly the linear extrapolation to zero field strength by least-squares fits. The first IP of all the actinide elements from Ac to Es with the exception of Pa have been determined with RIMS (Riegel *et al*., 1993; Trautmann, 1994; Deissenberger *et al*., 1995; Köhler *et al*., 1996, 1997; Erdmann *et al*., 1998; Peterson *et al*., 1998; Waldek *et al*., 2001). The results are summarized in Table 16.5 together with experimental data obtained by other methods and published in the literature (Solarz *et al*., 1976; Worden and Conway, 1979; Johnson *et al*., 1992; Worden *et al*., 1993) as well as with predictions from extrapolation of spectroscopic data (Sugar, 1974). The uncertainties of the RIMS values are statistical errors given as two standard deviations (2σ) derived from the least-squares fits including weighted errors for each data point.

An attempt to determine the first IP of Fm with 2 to 5×10^{10} atoms of ^{255}Fm ($t_{1/2} = 20.1$ h) with RIMS failed due to the short half-life of ^{255}Fm and the fact that no spectroscopic data for Fm were available. However, with a sandwich filament, where 2.7×10^{10} atoms of ^{257}Fm were electrodeposited on a Ta backing and covered with ~1 μm Ti, an atomic beam of Fm was produced at ~1000°C. The atoms were stored for ~40 ms in argon gas buffer-optical cell. They were resonantly excited and ionized with two beams of an excimer-dye consisting of a 200 Hz excimer pump laser that runs on XeF at wavelengths of 351/353 nm, and a one-step tunable dye laser. The resulting ions were identified after extraction from the optical cell with a quadrupole mass filter and a channeltron detector. Two atomic resonances of Fm were observed for the first time in this experiment at wavenumbers of 25099.80(4) cm^{-1} and 25111.80(4) cm^{-1}, and their lifetimes were estimated (Sewtz *et al*., 2003).

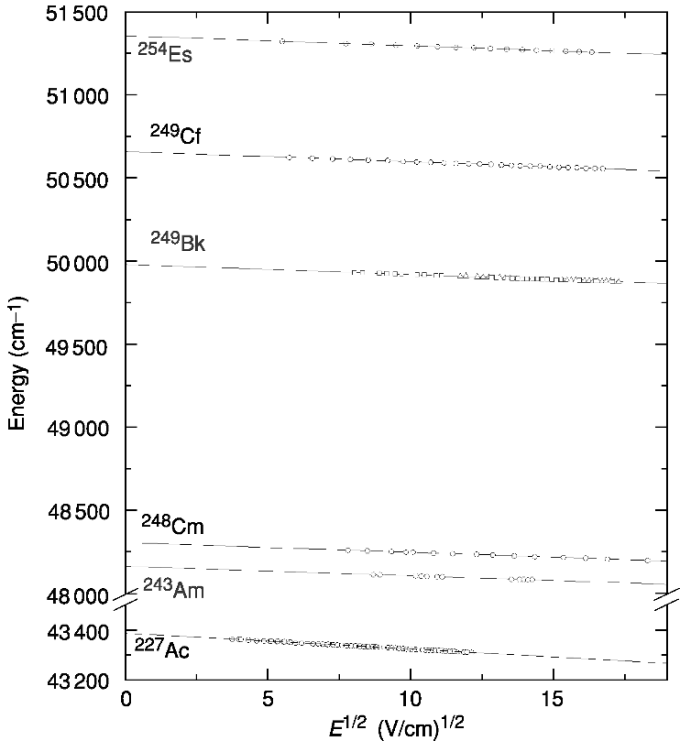

Fig. 16.10 *Plot of the measured ionization thresholds vs the square root of the electric field strength* E *for Ac, Am, Cm, Bk, Cf, and Es. Extrapolation to zero field strength yields the first IP. With this method, the first IPs of the six actinide elements shown here were determined experimentally for the first time.*

The ionization energies of the process $f^n s^2 \rightarrow f^n s$ were calculated by means of semiempirical Slater–Condon and *ab initio* HF calculations (Rajnak and Shore, 1978). For the lanthanides as well as for the actinides, the removal of an s-electron from the lowest $f^n s^2$ level producing an ion in the lowest $f^n s$ level is the most frequent mode of ionization in the f-series, and these ionization energies are called 'normalized IP–IP_n'. In all cases where the ground states differ from the configurations $f^n s^2$ and $f^n s$, corrections must be made by use of the known level energies of the lowest levels of the $f^n s^2$ and $f^n s$ configurations in the neutral and singly ionized atoms. In the lanthanide series (Worden *et al.*, 1978), it was observed that in a plot of IP_n versus n, the plot forms two straight lines connected at the half-filled shell ($n = 7$). The change in slope is interpreted as an effective exchange integral. A similar behavior is expected for the first IPs of the actinide elements.

In order to compare the experimental results with theoretical predictions (Sugar, 1974; Rajnak and Shore, 1978), the first IPs, normalized to

$5f^n7s^2 \rightarrow 5f^n7s$, are plotted versus the number of 5f electrons in Fig. 16.11. The experimental values of the heavier actinide elements are a little bit lower than the extrapolated data (Sugar, 1974) and slightly above the HF calculations (Rajnak and Shore, 1978). For the lighter actinides, the experimental IPs show strong deviations from the linear dependence, which might be connected to the fact that the ground states differ from f^ns^2 and most likely are due to CI. As pointed out (Rajnak and Shore, 1978), the actinide IPs should follow the trend for binding energies of the s-electrons by forming two straight lines, with a change of slope at Am, the half-filled f-shell. While the early actinides show considerable scatter, the higher actinides do follow the predicted behavior very well.

The high precision of RIMS in measuring the first IP of the actinides may also enable a determination of the isotope dependence of the IP, especially for elements which differ significantly in their neutron number, like ^{232}U and ^{238}U or ^{236}Pu and ^{244}Pu. The extension of the method to elements beyond Fm is difficult due to the limited amounts of material available and the short half-lives of the transfermium isotopes. For such investigations with online produced isotopes, an apparatus for RIMS in a buffer gas cell has been developed and might be suitable (Backe *et al.*, 1997). This method is based on resonance ionization in an argon buffer gas cell followed by ion-guide extraction and mass-selective direct detection of the resonantly ionized atoms.

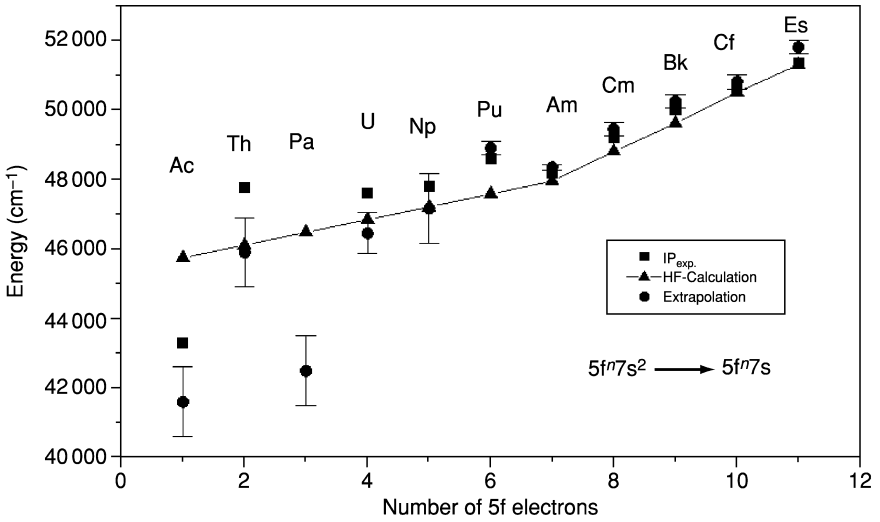

Fig. 16.11 *Comparison of the experimentally determined IPs of the actinides with two predictions* (*Sugar*, 1974; *Rajnak and Shore*, 1978). *The normalized first IPs* (IP_n) *are plotted for the ionization process* $5f^n7s^2 \rightarrow 5f^n7s$ *as a function of n, the number of 5f electrons. A straight line is drawn through the data from Hartree–Fock* (*HF*) *calculations* (*Rajnak and Shore*, 1978) (— ▲ —); *the values from extrapolated spectral properties* (*Sugar*, 1974) (●) *and the experimental data* $IP_{exp.}$ (▪) *are given with their errors.*

16.13 LASER SPECTROSCOPY OF SUPER-DEFORMED FISSION ISOMERS OF AMERICIUM

Fission isomers are interpreted as shape isomers (Bjornholm and Lynn, 1980; Metag *et al.*, 1980) corresponding to a second minimum in the potential energy surface (Strutinsky, 1967, 1968). The structure of the fission barrier with a double hump results from the superposition of shell corrections to the nuclear binding energy onto the rather flat maximum of the macroscopic part of the deformation energy as described by the liquid drop model. The double-humped fission barrier explains the basic features of fission isomers; e.g. their excitation energy of 2–3 MeV, their stability against γ-decay due to the inner barrier, and their short half-lives for spontaneous fission determined by the penetration of the outer barrier that is much smaller than the barrier for the spontaneous fission decay from the ground state. The fission isomers are mainly located in the actinide region and their half-lives are in the ps- to ms-range and thus 24–30 orders of magnitude shorter than those for spontaneous fission from the respective nuclear ground states.

The deformation parameter, the magnetic moment, and the nuclear spin can best be obtained by optical IS and hfs spectroscopy (Otten, 1989). These are valuable data for testing nuclear matter in the state of extreme deformation as is the case for fission isomers. A measurement of the IS allows the determination of the nuclear deformation parameter β_2. If the IS can be measured in chains of fission isomers, information on the stability of nuclear deformation as a function of the neutron number can be obtained. Furthermore, by resolved optical hyperfine spectroscopy, the intrinsic quadrupole moment, the nuclear spin, and the g-factor can be deduced. However, such experiments are not easy to perform due to the low production rate of fission isomers, on the order of a few per second and their very short half-lives ($t_{1/2} \leq 14$ ms).

Bemis and coworkers (Bemis *et al.*, 1979) provided the first direct experimental proof for the large deformation in ^{240f}Am ($t_{1/2} = 0.9$ ms) by laser spectroscopy. With the laser-induced nuclear polarization (LINUP) technique, they determined the relative IS ratio $IS^{240f/241}/IS^{243/241} = 26.8\ (20)$ by measuring the 640.5 nm optical transition ($^{10}P_{7/2} \rightarrow {}^{8}S_{7/2}$) for the isotopes ^{240f}Am, ^{241}Am, and ^{243}Am.

In order to extend the optical measurements on fission isomers, an ultrasensitive technique, radioactive-detected resonance ionization spectroscopy (RADRIS) in a buffer gas cell, has been developed (Backe *et al.*, 1992b, 1998) to perform hyperfine spectroscopy of fission isomers produced in heavy-ion-induced reactions. The method is based on resonance ionization in a buffer gas cell combined with radioactive decay detection and its feasibility was demonstrated with the β-active isotope ^{208}Tl (Lauth *et al.*, 1992). The first experiment on ^{242f}Am with the RADRIS technique was done at the Max-Planck-Institut für Kernphysik in Heidelberg (Backe *et al.*, 1992b). The experimental set-up is shown in Fig. 16.12. The ^{242f}Am fission isomers were produced via the reaction

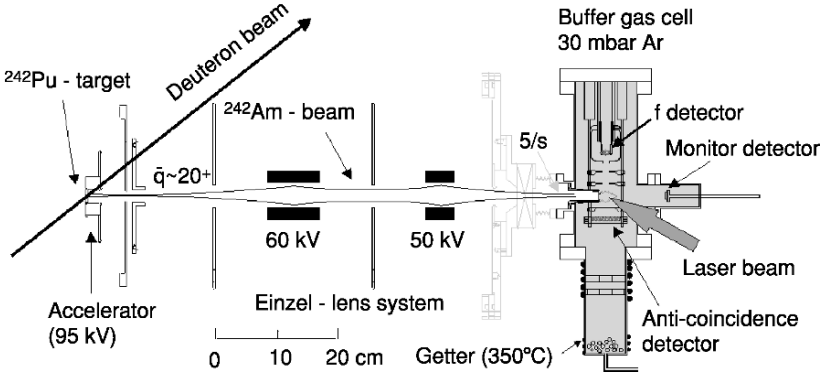

Fig. 16.12 *Experimental set-up for fission-detected resonance ionization spectroscopy in a buffer gas cell* (*Backe* et al., 1998). *For the production of* ^{242f}*Am a deuteron beam hits a* ^{242}*Pu-target and the fission isomers recoiling out of the target are accelerated and focused with an Einzel-lens system onto the entrance window of the optical buffer gas cell. The anti-coincidence fission detector is a PIN PD chip and the fission detector a windowless PIN photodiode. A dye laser and an excimer laser are used for resonance excitation and ionization. Getter techniques are applied to purify the gases.*

^{242}Pu (d,2n) ^{242f}Am by using a pulsed (5 ms on, 5 ms off) 12 MeV deuteron beam on a 50 μg/cm^2 $^{242}PuF_3$-target with a thin carbon backing. The fission isomers leaving the target have a recoil energy <100 keV and non-equilibrium ionic charge states between 10^+ and 35^+ (Metag *et al.*, 1980) as a result of conversion electron transitions followed by Auger cascades. After post-acceleration at a potential of 95 kV, the energy of the fission isomers was high enough to penetrate a 50 μg/cm^2 thick entrance window of the optical cell. On their way to the buffer gas cell, the fission isomers were focused with an Einzel-lens system. The ^{242f}Am beam at the entrance of the cell amounted typically to 5/s at a deuteron beam current of 5 μA. The optical cell, filled with 30 mbar argon and as quenching gas 0.3 mbar nitrogen, was loaded with the fission isomers during the beam-on periods. A fraction of ~15% of the recoiling ions was neutralized in the gas (Backe *et al.*, 1992a). The ions, not neutralized in the collision with the buffer gas, were fixed onto a thin electrode foil (250 μg/cm^2) in front of the anti-coincidence fission detector by applying an electric field. The gas acted as a storage medium for the neutral fission isomers. The diffusion time to the cell walls has been estimated to be ~30 ms. Resonance ionization was performed in the beam-off periods by two-color excitation/ionization. For this, an excimer laser (EMG 104 MSC, Lambda Physik) lasing with XeF at 351 and 353 nm for the second step and a dye laser (FL 2001, Lambda Physik) for the first excitation step were used. The resonantly ionized fission isomers were transported within 1.40(8) ms in an electric field of the ion electrode system to the fission detector. Fission events originating from isomers sticking on the foil

in front of the anti-coincidence detector or from neutrals in the gas phase were completely rejected by the signal, which the simultaneously emitted second fission fragment generated in the anti-coincidence detection. The bandwidth of the dye laser could be improved from 6 to 1.5 GHz by means of an intercavity etalon. Wavelength calibrations and the optimization of the laser system were performed in an off-line buffer gas cell with the long-lived α-active isotopes ^{243}Am and ^{241}Am (Backe *et al.*, 1993). During the online experiments, the wavelength of the dye laser was continuously monitored with absorption in Te_2 vapor (Cariou and Luc, 1980).

In addition to the fission isomer ^{242f}Am, the ^{240f}Am and ^{244f}Am fission isomers were produced. The reaction ^{242}Pu(p,3n) ^{240f}Am (σ = 10 μb) with a pulsed (2 ms on, 2 ms off) proton beam of 23 MeV energy (Backe *et al.*, 1998) produced the ^{240f}Am fission isomer. A 14 MeV deuteron beam on a ^{244}Pu target of 30 μg/cm^2 thickness (2 ms on, 2 ms off) was used to create the ^{244f}Am fission isomer with $t_{1/2}$ = 1.0 ms via the reaction ^{244}Pu (d,2n) ^{244f}Am (Backe *et al.*, 2000). The target consisted of $^{244}PuO_2$ (97.88% ^{244}Pu) on a thin carbon backing (34 μg/cm^2).

Most of the measurements were done with ^{242f}Am. The IS of ^{242f}Am has been measured for three optical transitions for which the IS values IS$^{243/241}$ between the ^{243}Am and ^{241}Am isotopes are known (Worden, 1991–1993; Blaise and Wyart, 1992). The initial IS measurement was performed at λ_1 = 468.17 nm (Backe *et al.*, 1992b, 1993). An IS$^{242f/241}$ (468 nm) = –1.18(9) cm^{-1} was determined, corresponding to an IS ratio IS$^{242f/241}$/IS$^{243/241}$ = 24.6(24) using IS$^{243/241}$ = 0.048(3) cm^{-1} for this wavelength. A second measurement (Backe *et al.*, 1998) with λ_1 = 499.08 nm yielded an IS$^{242f/241}$ (499 nm) = +2.83(9) cm^{-1} and an isotope ratio IS$^{242f/241}$/IS$^{243/241}$ = 44.9(26) with IS$^{243/241}$ (499 nm) = 0.063(3) cm^{-1}. The disagreement of the two isotope ratio values originates from an anomaly in the 468.17 nm transition caused by configuration mixing. The same explanation can be given for the disagreement with the ~41 value and the value of 26.8 obtained by Bemis *et al.* at the 640.5 nm transition. The configuration mixing is between the 15608 cm^{-1} level and a level at 15273 cm^{-1} of the same parity and J with a large IS of opposite sign. A third measurement (Backe *et al.*, 1996, 1998) at λ_1 = 500.02 nm resulted in an IS$^{242f/241}$ (500 nm) = +10.358(14) cm^{-1}. The isotope ratio of IS$^{242f/241}$/IS$^{243/241}$ = 41.4(8) was obtained with IS$^{243/241}$ = 0.250(5) cm^{-1} in good agreement with the value at λ_1 = 499.08 um.

The IS measurements of ^{240f}Am at the 500 nm transition (Backe *et al.*, 1998) delivered a resonance signal just 0.56 cm^{-1} away from the one of ^{242f}Am. The IS$^{240f/241}$ = 9.80(3) cm^{-1} corresponds to an IS ratio IS$^{240f/241}$/IS$^{243/241}$ = 39.2(8). The IS of ^{244f}Am relative to ^{241}Am at a wavelength of 500 nm was determined to be IS$^{244f/241}$ = 10.49(4) cm^{-1}, with a signal very close to ^{240f}Am and ^{242f}Am, which gives an IS ratio IS$^{244f/241}$/IS$^{241/243}$ = 42.0(9) (Backe *et al.*, 2000, 2001). Fig. 16.13 summarizes the resonance ionization signals at the 500.02 nm transition of the fission isomers ^{244f}Am, ^{242f}Am and ^{240f}Am relative to ^{241}Am.

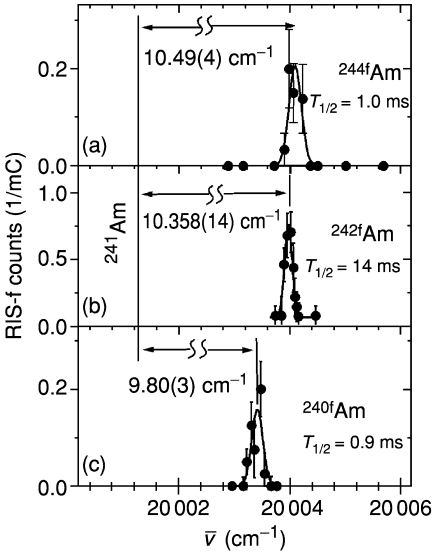

Fig. 16.13 *Resonance ionization signals of the fission isomers* ^{244f}*Am* (*a*), ^{242f}*Am* (*b*), *and* ^{240f}*Am* (*c*) *at the* 500.02 nm *transition* (*Backe* et al., 2001). *The IS values to the reference isotope* ^{241}*Am are indicated.*

Table 16.7 *Isotope shifts* $IS^{24xf/241}$, *IS ratios* $IS^{24xf/241}/IS^{243/241}$, *and nuclear parameters* $\lambda^{24xf/241}$ *for the fission isomers* ^{240f}*Am,* ^{242f}Am, and ^{244f}*Am. The measurements were performed at the* 500 nm *transition. The deformation parameters* β_2 *and the quadrupole moments* Q_{20} *have been calculated with the deformed droplet model* (*Backe* et al., 2001).

Isomer	$IS^{24xf/241}$ (cm^{-1})	$IS^{24xf/241}/IS^{243/241}$	$\lambda^{24xf/241}$ (fm^2)	β_2	Q_{20} (eb)
^{240f}Am	9.80(3)	39.2(8)	5.06(30)	0.690	33.9
^{242f}Am	10.358(14)	41.4(8)	5.34(28)	0.699	34.5
^{244f}Am	10.49(4)	42.0(9)	5.41(31)	0.694	34.4

In the determination of the deformation of the fission isomeric states, the mass shift contributions were neglected because the normal mass shift is only 0.004% of the measured IS of the fission isomers. The deformation parameters β_2 and the intrinsic quadrupole moments Q_{20} of the fission isomeric states have been evaluated (Backe *et al.*, 1998) on the basis of the droplet model (Meyers and Schmidt, 1983) and from the nuclear parameters employing a charge distribution of the deformed Fermi model (Brack *et al.*, 1974) with the assumption that the IS between ^{243}Am and ^{241}Am comes from a pure nuclear volume change. The results obtained with the deformed droplet model are presented in Table 16.7 for the three fission isomers of Am. In the analysis, a hexadecapole parameter $\beta_4^{II} = 0.08$ has been assumed, which is a theoretical prediction value

(Howard and Möller, 1980). The small differences of the nuclear charge parameters of the three fission isomers (e.g. $\Lambda^{244f/242f} = 0.069(21)$ fm^2) result in small changes of the deformation parameters β_2 and the quadrupole moments Q_{20}, as can be seen from Table 16.7.

Precise IS measurements are now available for the fission isomers ^{240f}Am, ^{242f}Am, and ^{244f}Am obtained with the fission RADRIS method in a buffer gas cell at very low production rates of ~5/s. The results demonstrate the stability of the deformation in the second potential minimum if neutron pairs are added in accordance with earlier calculations (Howard and Möller, 1980). The experimentally determined deformation parameters are a little bit larger than the theoretically calculated value $\beta_2 = 0.61$ (Howard and Möller, 1980). The laser spectroscopic method corroborates independently the charge plunger measurements (Metag *et al.*, 1980) and confirms the extreme deformation of fission isomers. To illustrate this, Fig. 16.14 shows the quadrupole moments of fission isomers and nuclear ground states for the lighter actinides. First hyperfine spectroscopic measurements, required for the determination of the nuclear spin and the *g*-factor, have been performed at the 466.28 nm transition of ^{242f}Am (Backe *et al.*, 1996). From the obtained data, a negative *g*-factor and a spin of $I = 2$–3 were derived (Lauth *et al.*, 1998). However, more detailed deformed shell-model calculations are required for the interpretation of the measured *g*-factor of ^{242f}Am. In addition to the results obtained with resonance ionization spectroscopy in a buffer gas cell, this method should also be applicable for studies of the atomic and nuclear properties of transeinsteinium elements (Backe *et al.*, 1997; Sewtz *et al.*, 2003).

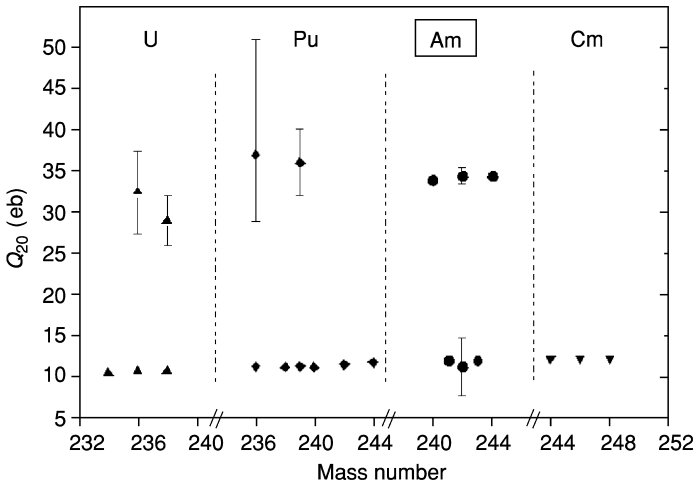

Fig. 16.14 *Quadrupole moments* Q_{20} *in the actinide region for the nuclear ground state and for the fission isomeric state.*

APPENDIX 16.1 THE CONSTRUCTION OF Es ELECTODELESS LAMPS

The design and construction of the EDL was modified when amounts of ~100 μg or more of Es became available because of the poor yields (<15%) obtained with no carrier element present (Worden *et al.*, 1968, 1970, and especially Worden *et al.*, 1974). The vacuum system used to prepare the pure Es lamps is shown in Fig. A16.1. A 6 mm outer diameter (o.d.) quartz frit was used to collect and wash ~100 μg of Es oxalate precipitated from a recently purified Es solution taken from a resin column. The high specific activity (5.6×10^{10} alpha activity per min per microgram) of ~100 μg of Es prevented collecting and washing of the precipitate in the usual 6 mm o.d. cone (because the intense alpha activity stirred up the solid) as done in normal lamp preparation. The quartz frit was inserted into reaction tube (at this point not sealed to the vacuum system as shown in Fig. A16.1) and the Es oxalate converted to Es_2O_3 by heating with a torch to red heat in the quartz frit with air present. The constriction at B was then made with a torch while holding the reaction tube vertical. The reaction tube was then turned horizontal and sealed to the Pyrex system at A in Fig. A16.1.

The assembly was pumped down to high vacuum ($<10^{-3}$ Pa) and the entire quartz part of the assembly was out-gassed with a tube furnace at ~1000°C. The thin capillary containing the AlI_3 was moved so that the iron slugs could break the tip using external magnets. Then the capillary assembly was moved so that the tip of the capillary was inside the reaction tube at constriction B. The AlI_3 was then sublimed into the reaction tube with a torch. The Es material and sublimed AlI_3 reactant and the final lamp were sealed off together at point B under high vacuum. The reaction at 560°C was carried out in a tube furnace with the reaction tube and lamp blank contained in a stainless steel tube with a

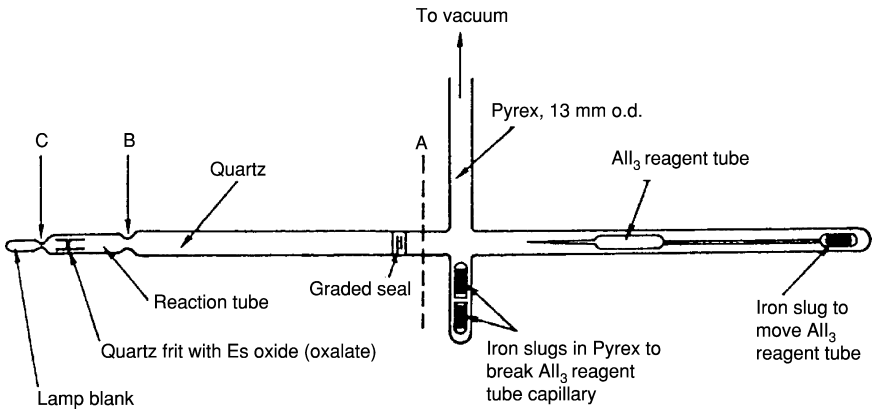

Fig. A16.1 *Vacuum apparatus for the preparation of einsteinium electrodeless lamps.*

sealed screw top for about 3 h. The stainless steel tube was cooled and the reaction tube and lamp blank removed. The product EsI_3 plus the excess AlI_3 was sublimed at ~750–800°C into the lamp blank cooled with wet asbestos cloth on the end of the lamp. The oven temperature was then reduced to ~500°C and the AlI_3 and other high vapor pressure impurities were sublimed into the reaction tube cooled with wet asbestos cloth. The lamp was then separated from the reaction tube at point C using a torch with wet asbestos cloth covering the lamp and reaction tube. This produced a lamp with up to 90% of the Es in the lamp, but also many impurities. The lamp life was about the same as lamps of other actinides prepared by the standard technique.

These procedures for the pure Es lamps were carried out at ANL so the time from purification of the 20.5 day half-life ^{253}Es to observation of the spectrum on the ANL spectrograph was reduced. The minimum time for the process was reduced to about 12 h vs the previous times of 2–3 days.

ACKNOWLEDGMENTS

This work was performed in part under the auspices of the U.S. Department of Energy by University of California, Lawrence Livermore National Laboratory under Contract W-7405-Eng-48. This document was prepared as an account of work sponsored by an agency of the United States Government. Neither the United States Government nor the University of California nor any of their employees, makes any warranty, express or implied, or assumes any legal liability or responsibility for the accuracy, completeness, or usefulness of any information, apparatus, product, or process disclosed, or represents that its use would not infringe privately owned rights. Reference herein to any specific commercial product, process, or service by trade name, trademark, manufacturer, or otherwise, does not necessarily constitute or imply its endorsement, recommendation, or favoring by the United States Government or the University of California. The views and opinions of authors expressed herein do not necessarily state or reflect those of the United States Government or the University of California, and shall not be used for advertising or product endorsement purposes.

LIST OF ABBREVIATIONS

ANL	Argonne National Laboratory
AVLIS	Atomic Vapor Laser Isotope Separation
EDL	electrodeless discharge lamp
FTS	Fourier Transform Spectrometers
GLS	generalized-least-squares
hfs	hyperfine structure
IP	ionization potential
IS	isotope shifts

LAC	Laboratoire Aimé Cotton
LINUP	laser-induced nuclear polarization
LLNL	Lawrence Livermore National Laboratory
NIST	National Institute of Standards and Technology
RADRIS	radioactive-detected resonance ionization spectroscopy
RIMS	resonance ionization mass spectroscopy
TOF	time of flight

REFERENCES

Avril, R., deLabachellerie, M., Viala, F., and Petit, A. (1986) *J. Less Common Metals,* **122**, 47–53.

Avril, R., Ginibre, A., and Petit, A. (1994) *Z. Phys. D,* **29**, 91–102.

Backe, H., Lauth, W., Achenbach, W., Hain, M., Hies, M., Scherrer, A., Steinhof, A., Tölg, S., and Ziegler, S. (1992a) *Nucl. Instrum. Methods Phys. Res.,* **B70**, 521–31.

Backe, H., Blönningen, Th., Dahlinger, M., Doppler, U., Graffé, P., Habs, D., Hies, M., Illgner, Ch., Kunz, H., Lauth, W., Schöpe, H., Schwamb, P., Theobald, W., and Zahn, R. (1992b) *Hyperfine Interact.,* **74**, 47–57.

Backe, H., Graffé, P., Habs, D., Hies, M., Illgner, Ch., Kunz, H., Lauth, W., Schöpe, H., Schwamb, P., Theobald, W., Thörle, P., Trautmann, N., and Zahn, R. (1993) *Hyperfine Interact.,* **78**, 35–45.

Backe, H., Baum, R.-R., Fricke, B., Habs, D., Hellmann, K., Hies, M., Illgner, Ch., Krameyer, Ch., Kunz, H., Lauth, W., Martin, R., Schwamb, P., Theobald, W., Thörle, P., and Trautmann, N. (1996) *Hyperfine Interact.,* **97/98**, 535–41.

Backe, H., Eberhardt, K., Feldmann, R., Hies, M., Kunz, H., Lauth, W., Martin, R., Schöpe, H., Schwamb, P., Sewtz, M., Thörle, P., Trautmann, N., and Zauner, S. (1997) *Nucl. Instrum. Methods Phys. Res.,* **B126**, 406–10.

Backe, H., Hies, M., Kunz.,H., Lauth, W., Curtze, O., Schwamb, P., Sewtz, M., Theobald, W., Zahn, R., Eberhardt, K., Trautmann, N., Habs, D., Repnow, R., and Fricke, B. (1998) *Phys. Rev. Lett.,* **80**, 920–3.

Backe, H., Dretzke, A., Hies, M., Kube, G., Kunz, H., Lauth, W., Sewtz, M., Trautmann, N., Repnow, R., and Maier, H. J. (2000) *Hyperfine Interact.,* **127**, 35–9.

Backe, H., Dretzke, A., Habs, D., Hies, M., Kube, G., Kunz, H., Lauth, W., Maier, H. J., Repnow, R., Sewtz, M., and Trautmann, N. (2001) *Nucl. Phys.,* **A690**, 215c–18c.

Bauche-Arnoult, C., Gerstenkorn, S., Verges, J., and Tomkins, F. S. (1973) *J. Opt. Soc. Am.,* **63**, 1199–203.

Bauche, J., Blaise, J., and Fred, M. (1963a) *C. R. Acad. Sci. Paris*, **256**, 5091–3.

Bauche, J., Blaise, J., and Fred, M. (1963b) *C. R. Acad. Sci. Paris*, **257**, 2260–3.

Bemis, C. E. Jr, Beene, J. R., Young, J. P., and Kramer, S. D. (1979) *Phys. Rev. Lett.,* **43**, 1854–8.

Bjornholm, S. and Lynn, J. E. (1980) *Rev. Mod. Phys.,* **52**, 725–931.

Blaise, J., Fred, M., Gerstenkorn, S., and Judd, B. R. (1962) *C. R. Acad. Sci. Paris*, **255**, 2403–5.

Blaise, J. and Radziemski, L. J. Jr (1976) *J. Opt. Soc. Am.,* **66**, 644–59.

Blaise, J., Luc, P., and Verges, J. (1977) *9th EGAS Conf*., Cracow.

Blaise, J., Wyart, J.-F., Conway, J. G., and Worden, E. F. (1980) *Phys. Scr.,* **22**, 224–30.
Blaise, J., Verges, J., Wyart, J.-F., Conway, J. G., and Worden, E. F. (1981) *Eur. Conf At. Phys.*, Heidelberg, vol. 5A, part I, pp. 102–3.
Blaise, J., Fred, M., Carnall, W. T., Crosswhite, H. M., and Crosswhite, H. (1983) *Plutonium Chemistry* (ACS Symp. Ser. no. 216), American Chemical Society, Washington DC, pp. 173–98.
Blaise, J., Wyart, J.-F., Palmer, B. A., and Engleman, R. Jr (1984a) *16th EGAS Conf.*, London.
Blaise, J., Fred, M., and Gutmacher, R. G. (1984b) Argonne National Laboratory Report ANL-83–95.
Blaise, J., Ginibre, A., and Wyart, J.-F. (1985) *Z. Phys. A. Atoms and Nuclei***, 321**, 61–3.
Blaise, J., Fred, M., and Gutmacher, R G. (1986) *J. Opt. Soc. Am. B*, 3, 403–18.
Blaise, J., Wyart, J.-F., Palmer, B. A., Engleman, R. Jr, and Launay, F. (1987) *19th EGAS Conf.*, Dublin, Europhys. Conf. Abstracts **11E**, A3–08.
Blaise, J., Wyart, J.-F., Engleman, R. J., and Palmer, B. A. (1988a) *J. Opt. Soc. Am. B,* **5**, 2087–92.
Blaise, J., Worden, E. F., and Conway, J. G. (1988b) *J. Opt. Soc. Am. B***, 5**, 2093–106.
Blaise, J. and Wyart, J.-F. (1992) *Energy Levels and Atomic Spectra of Actinides*. Tables Internationales de Constantes Sélectionées, Université Pierre et Marie Curie, Paris, vol. 20.
Blaise, J., Wyart, J.-F., Verges, J., Engleman, R. Jr, Palmer, B. A., and Radziemski, L. J. Jr (1994) *J. Opt. Soc. Am. B***, 11**, 1897–929.
Blaise, J., Worden, E. F., and Wyart, J.-F. (2003) analysis in progress.
Bordarier, Y. (1970) Thesis, University of Paris; Bordarier, Y., Bachelier, A., Sinzelle, J., computer codes (unpublished).
Brack, M., Ledergerber, T., Pauli, H. C., and Jensen, A. S. (1974) *Nucl. Phys. A,* **234**, 185–215.
Brault, J. W. (1976) *J. Opt. Soc. Am.,* **66**, 1081A.
Brewer, L. (1984) *High Temp. Sci.,* **17**, 1–30; (1971) *J. Opt. Soc. Am.*, **61**, 1101–11; 1666–82.
Cariou, J. and Luc, P. (1980) *Atlas du Spectre d'Absorption de la Molecule Tellure*, Laboratoire Aimé Cotton, CNRS II, Orsay, France.
Carnall, W. T., Crosswhite, H., and Crosswhite, H. M. (1978) *Energy Level Structure and Transition Probabilities of the Trivalent Lanthanides in* LaF_3, Argonne National Laboratory Report ANL-78-77.
Childs, W. J., Poulsen, O., and Goodman, L. S. (1979a) *Opt. Lett.,* **4**, 35–7.
Childs, W. J., Poulsen, O., and Goodman, L. S. (1979b) *Opt. Lett.,* **4**, 63–5.
Condon, E. U. and Shortley, G. H. (1935) *The Theory of Atomic Spectra*, Cambridge University Press, Cambridge, ch. VI.
Connes, J., Delouis, H., Connes, P., Guelachvili, G., Maillard, J.-P., and Michel, G. (1970) *Nouv. Rev. Opt. Appl. Fr.,* **1**, 3–22.
Conway, J. G., Blaise, J., and Verges, J. (1976) *Spectrochim. Acta B,* **31**, 31–47.
Conway, J. G., Worden, E. F., Blaise, J., and Verges, J. (1977a) *Spectrochim. B. Acta***, 32**, 97–9.
Conway, J. G., Worden, E. F., Blaise, J., Camus, P., and Verges, J. (1977b) *Spectrochim. Acta B***, 32**, 101–6.

Conway, J. G., Worden, E. F., Brault, J. W., Hubbard, R. P., and Wagner, J. J. (1984) *At. Data Nud. Data Tables*, **31**, 299–358

Conway, J. G., Worden, E. F., and Blaise, J. (1995) *J. Opt. Soc. Am. B,* **12**, 1186–202.

Coste, A., Avril, R., Blancard, P., Chatelet, J., Lambert, D., Legre, J., Liberman, S., and Pinard, J. (1982) *J. Opt. Soc. Am.,* **72**, 103–9.

Cowan, R. D. (1968) *J. Opt. Soc. Am.,* **58**, 808–18.

Cowan, R. D. (1981) *The Theory of Atomic Structure and Spectra*, University of California Press, Berkeley, CA.

Crosswhite, H. M. (1971) *Phys. Rev. A,* **4**, 485–9.

Crosswhite, H. M. (1975) Private communication to M. Fred.

Crosswhite, H. M. (1986) Private communication.

Deissenberger, R., Köhler, S., Ames, F., Eberhardt, K., Erdmann, N., Funk, H., Herrmann, G., Kluge, H.-J., Nunnemann, M., Passler, G., Riegel, J., Scheerer, F., Trautmann, N., and Urban, F.-J. (1995) *Angew. Chem. Int. Ed. Engl.,* **34**, 814–15.

Demers, Y., Gagne, J. M., Dreze, C., and Pianarosa, P. (1986) *J. Opt. Soc. Am. B,* **3**, 1678–80.

Engleman, R. Jr and Palmer, B. A. (1980) *J. Opt. Soc. Am.,* **70**, 308–17.

Engleman, R. Jr and Palmer, B. A. (1983) *J. Opt. Soc. Am.,* **73**, 694–701

Engleman, R. Jr and Palmer, B. A. (1984) *J. Opt. Soc. Am. B*, **1**, 782–7.

Erdmann, N., Nunnemann, M., Eberhardt, K., Herrmann, G., Huber, G., Köhler, S., Kratz, J. V., Passler, G., Peterson, J. R., Trautmann, N., and Waldek, A. (1998) *J. Alloys Compds,* **271–273**, 837–40.

Feneuille, S. and Pelletier-Allard, N. (1968) *Physica,* **40**, 347–56.

Fred, M. and Tomkins, F. S. (1957) *J. Opt. Soc. Am.,* **47**, 1076–87.

Fred, M., Tomkins, F. S., Blaise, J., Camus, P., and Verges, J. (1976) Argonne National Laboratory Report ANL-76-68.

Fred, M., Tomkins, F. S., Blaise, J., Camus, P., and Verges, J. (1977) *J. Opt. Soc. Am.,* **67**, 7–23.

Fred, M. and Blaise, J. (1978) private communication of the 0.00 to 24.27 cm^{-1} low level separation in Np(II).

Fricke, B., Johnson, E., and Rivera, G. M. (1993) *Radiochimica Acta,* **62**, 17–25.

Giacchetti, A. (1966) *J. Opt. Soc. Am.,* **56**, 653–7.

Giacchetti, A. (1967) *J. Opt. Soc. Am.,* **57**, 728–33.

Giacchetti, A. and Blaise, J. (1970) *2nd EGAS Conf.*, Hanover.

Giacchetti, A., Blaise, J., Corliss, C. H., and Zalubas, R. J. (1974) *J. Res. NBS,* **78A**, 247–81.

Goeppert Mayer, M. (1941) *Phys. Rev.,* **60**, 184–7.

Goldschmidt, Z. B. (1983) *Phys. Rev. A,* **27**, 740–53.

Greenland, P. T., Pritchard, S. E., and Wort, D. J. H. (1981) Poster AERE Harwell OX11 ORA.

Grüning, C., Huber, G., Klopp, P., Kratz, J. V., Kunz, P., Passler, G., Trautmann, N., Waldek, A., and Wendt, K. (2004) *Int. J. Mass Spectrometry*, **235**, 171–8.

Gutmacher, R. G., Evans, J. E., and Hulet, E. K. (1967) *J. Opt. Soc. Am.,* **57**, 1389–90.

Hackel, L. A., Bender, C. A., Johnson, M. A., and Rushford, M. A. (1979) *J. Opt. Soc. Am.,* **69**, 230–2.

Hansen, J. E., Judd, B. R., and Crosswhite, H. (1996) *At. Data Nuc. Data Tables,* **62**, 1–49.

Howard, W. M. and Möller, P. (1980) *At. Data Nucl. Data Tables,* **25**, 219–85.
Hulet, E. K., Lougheed, R. W., Brady, J. D., Stone, R. E., and Coops, M. S. (1967) *Science,* **158**, 486–8.
Johnson, S. G., Fearey, B. L., Miller, C. M., and Nogar, N. S. (1992) *Spectrochim. Acta B,* **47**, 633–43.
Judd, B. R. (1963) *Operator Techniques in Atomic Spectroscopy*, Wiley Interscience, New York.
Judd, B. R. (1966) *Phys. Rev.,* **141**, 4–14.
Judd, B. R. and Crosswhite, H. M. (1984) *J. Opt. Soc. Am. B,* **1**, 255–60.
Judd, B. R. (1985) *Rep. Prog. Phys.,* **48**, 907–54.
Judd, B. R. and Lo, E. (1996) *At. Data Nucl. Data Tables,* **62**, 51–75.
Kaufman, V. and Radziemski, L. J. Jr (1976) *J. Opt. Soc. Am.,* **66**, 599–600.
Klinkenberg, P. F. A. and Lang, R. G. (1949) *Physica,* **15**, 774–88.
Klinkenberg, P. F. A. (1950) *Physica,* **16**, 618–50.
Klinkenberg, P. F. A. and Uylings, P. H. M. (1986) *Phys. Scr.,* **34**, 413–22.
Klinkenberg, P. F. A. (1988) *Physica***, 151**, 552–67.
Köhler, S., Erdmann, N., Nunnemann, M., Herrmann, G., Huber, G., Kratz, J. V., Passler, G., and Trautmann, N. (1996) *Angew. Chem. Int. Ed. Engl.,* **35**, 2856–8.
Köhler, S., Deißenberger, R., Eberhardt, K., Erdmann, N., Herrmann, G., Huber, G., Kratz, J. V., Nunnemann, M., Passler, G., Rao, P. M., Riegel, J., Trautmann, N., and Wendt, K. (1997) *Spectrochim. Acta B,* **52**, 717–26.
Kramida, A. E. (1997) PC version of the RCN/RCG/RCE Cowan codes available on the web site plasma-gate@weizmann.ac.il
Lauth, W., Backe, H., Dahlinger, M., Klaft, I., Schwamb, P., Schwickert, G., Trautmann, N., and Othmer, U. (1992) *Phys. Rev. Lett.,* **68**, 1675–8.
Lauth, W., Backe, H., Hies, M., Kolb, T., Kunz, H., Schütze, Th., Sewtz, M., Steinhof, A., Eberhardt, K., Trautmann, N., and Repnow, R. (1998) in *Heavy Ion Physics* (eds. Yu. Ts. Oganessian and R. Kalpakchieva) World Scientific Publishing, Singapore, pp. 588–97.
Le Garrec, B. and Petit, A. (1986) *J. Less Common Metals,* **122**, 55–8.
Litzen, U. (1974) *Phys. Scr.,* **10**, 103–4.
Lobikov, E. A., Striganov, A. R., Labozin, V. P., Odintsova, N. K., and Pomytkin, V. F. (1979) *Opt. Spekctrosk.,* **46**, 1054–60; *Opt. Spectrosc.*, **46**, 596–9.
Marrus, R., Nierenberg, W. A., and Winocur, J. (1960) *Phys. Rev.,* **120**, 1429–35.
McNally, J. R. Jr and Griffin, P. M. (1959) *J. Opt. Soc. Am.,* **49**, 162–6.
Meggers, W. F., Fred, M., and Tomkins, F. S. (1957) *J. Res. NBS,* **58**, 297–315.
Meisel, G., Bekk, K., Rebel, H., and Schatz, G. (1987) *Hyperfine. Interact.,* **38**, 723–40.
Metag, V., Habs, D., and Specht, H. J. (1980) *Phys. Rep.,* **65**, 1–41.
Meyers, W. D. and Schmidt, K. H. (1983) *Nucl. Phys. A,* **410**, 61–73.
Morss, L. R. (1971) *J. Phys. Chem.,* **75**, 392–9.
Nielson, C. W. and Koster, G. F. (1964) *Spectroscopic Coefficients for p^n, d^n, and f^n Configurations*, MIT Press, Cambridge, MA.
Nugent, L. J. (1975) *MTP International Review of Science, Inorganic Chemistry*, sec. 2, vol. 7, Butterworths, London, pp. 195–219.
Otten, E. W. (1989) *Treatise on Heavy-Ion Science*, Plenum, vol. 8.
Palmer, B. A., Keller, R. A., and Engleman, R. Jr (1980) *An Atlas of Uranium Emission Intensities in a Hollow Cathode Discharge*, Los Alamos Scientific Laboratory Report LA-8251-MS.

Palmer, B. A. and Engleman, R. Jr (1983) *Atlas of the Thorium Spectrum*, Los Alamos National Laboratory Report LA-9615.
Palmer, B. A. and Engleman, R. Jr (1984) *J. Opt. Soc. Am. B*, **1**, 782–7.
Peterson, J. R., Erdmann, N., Nunnemann, M., Eberhardt, K., Huber, G., Kratz, J. V., Passler, G., Stetzer, O., Thörle, P., Trautmann, N., and Waldek, A. (1998) *J. Alloys Compds,* **271–273**, 876–8.
Petit, A. (1999) *Eur. Phys. J. D,* **6**, 157–70.
Pulliam, B. V. (1985) private communication to J. Blaise.
Pulliam, B. V., Conway, J. G., and Worden, E. F. (2003) unpublished results.
Pyykkö, P. and Desclaux, J. P. (1979) *Acc. Chem. Res.,* **12**, 276–81.
Pyykkö, P. (1988) *Chem. Rev.,* **88**, 563–94.
Racah, G. (1942) *Phys. Rev.,* **62**, 438–62.
Racah, G. (1943) *Phys. Rev.,* **63**, 367–82.
Racah, G. (1949) *Phys. Rev.,* **76**, 1352–65.
Racah, G. (1950) *Physica,* **16**, 651–66.
Racah, G. (1951) *Bull. Res. Counc. Isr.,* **8F**, 1–14.
Rajnak, K. and Wybourne, B. G. (1964) *Phys. Rev. A,* **134**, 596–600.
Rajnak, K. and Fred, M. (1977) *J. Opt. Soc. Am.,* **67**, 1314–23.
Rajnak, K. and Shore, B. W. (1978) *J. Opt. Soc. Am.,* **68**, 360–7.
Rajnak, K. (1979) private communication to M. Fred.
Reader, J. and Corliss, C. H. (1980) *Wavelengths and Transition Probabilities for Atoms and Atomic Ions, Part I, Wavelengths,* NSRDS-NBS 68, Washington DC.
Riegel, J., Deissenberger, R., Herrmann, G., Köhler, S., Sattelberger, P., Trautmann, N., Wendeler, H., Ames, F., Kluge, H.-J., Scheerer, F., and Urban, F.-J. (1993) *Appl. Phys.,* **B56**, 275–80.
Rudzikas, Z. (1997) *Theoretical Atomic Spectroscopy*, Cambridge University Press, Cambridge, England.
Ruster, W., Ames, F., Kluge, H.-J., Otten, E.-W., Rehklau, D., Scheerer, F., Herrmann, G., Mühleck, C., Riegel, J., Rimke, H., Sattelberger, P., and. Trautmann, N. (1989) *Nucl. Instrum. Methods Phys. Res. A,* **281**, 547–58.
Sewtz, M. H., Backe, A., Dretzke, G., Kube, W., Lauth, P., Schwamb, K., Eberhardt, C., Grüning, P., Thörle, P., Trautmann, N., Kunz, P. J., Lassen, G., Passler, G., Dong, C. Z., Fritsche, S., and Haire, R. G. (2003) *Phys. Rev. Lett.,* **90**, 163002–1-4.
Slater, J. C. (1929) *Phys. Rev.*, **34**, 1293–322.
Slater, J. C. (1960) *Quantum Theory of Atomic Structure*, vol. I, McGraw-Hill, New York.
Solarz, R. W., May, C. A., Carlson, L. R., Worden, E. F., Johnson, S. A., Paisner, J. A., and Radziemski, L. J. Jr (1976) *Phys. Rev. A,* **14**, 1129–36.
Steinhaus, D. W., Radziemski, L. J. Jr, Cowan, R. D., Blaise, J., Guelachvili, G., Ben Osman, Z., and Verges, J. (1971) Los Alamos Scientific Laboratory Report LA-4501.
Striganov, A. R. (1983) *Atomic Spectrum and Energy Levels of the Neutral Atom of Plutonium*, Energoatomisdat, Moscow (in Russian).
Strutinsky, V. M. (1967) *Nucl. Phys.,* **A95**, 420–42.
Strutinsky, V. M. (1968) *Nucl. Phys.,* **A122**, 1–33.
Sugar, J. (1974) *J. Chem. Phys.,* **60**, 4103.
Tomkins, F. S. and Fred, M. (1951) *J. Opt. Soc. Am.,* **41**, 641–3.
Tomkins, F. S. and Fred, M. (1957) *J. Opt. Soc. Am.,* **47**, 1087–91.
Tomkins, F. S. and Fred, M. (1963) *Appl. Opt.,* **2**, 715–25.

Trautmann, N. (1994) *J. Alloys Compds,* **213–214**, 28–32.
Van Deurzen, C. H. H., Rajnak, K., and Conway, J. G. (1984) *J. Opt. Soc. Am. B,* **1**, 45–7.
Vander Sluis, K. L. and Nugent, L. J. (1972) *Phys. Rev. A,* **6**, 86–94.
Waldek, A., Erdmann, N., Grüning, C., Huber, G., Kunz, P., Kratz, J. V., Lassen, J., Passler, G., and Trautmann, N. (2001) *Resonance Ionization Spectroscopy 2000* (eds. J. E. Parks and J. P. Young), AIP Conf. Proc., 584, American Institute of Physics, Melville, NY, 219–24.
White, H. E. (1934) *Introduction to Atomic Spectra*, McGraw-Hill, New York, p. 441
Wilson, M. (1968) *Phys. Rev.,* **176**, 58–63.
Worden, E. F., Gutmacher, R. G., and Conway, J. G. (1963) *Appl. Opt.,* **2**, 707–13.
Worden, E. F. and Conway, J. G. (1967) *Physica*, **33**, 274.
Worden, E. F., Hulet, E. K., Lougheed, R. M., and Conway, J. G. (1967) *J. Opt. Soc. Am.,* **57**, 550.
Worden, E. F., Gutmacher, R. G., Lougheed, R. W., Evans, J. E., and Conway, J. G. (1968) *J. Opt. Soc. Am.,* **58**, 998–9.
Worden, E. F. and Conway, J. G. (1970) *J. Opt. Soc. Am.,* **60**, 1144–5.
Worden, E. F., Gutmacher, R. G., Lougheed, R. W., Conway, J. G., and Mehlhorn, R. J. (1970) *J. Opt. Soc. Am.,* **60**, 1297–302.
Worden, E. F., Lougheed, R. W., Gutmacher, R. G., and Conway, J. G. (1974) *J. Opt. Soc. Am.,* **64**, 77–85.
Worden, E. F., Hulet, E. K., Gutmacher, R. G., and Conway, J. G. (1976) *At. Data Nucl. Data Tables***, 18**, 459–95.
Worden, E. F. and Conway, J. G. (1976) *J. Opt. Soc. Am.,* **66**, 109–21.
Worden, E. F. and Conway, J. G. (1978) *At. Data Nucl. Data Tables***, 22**, 329–66.
Worden, E. F., Solarz, R. W., Paisner, J. A., and Conway, J. G. (1978) *J. Opt. Soc. Am.,* **68**, 52–61.
Worden, E. F. and Conway, J. G. (1979) *J. Opt. Soc. Am.,* **69**, 733–8.
Worden, E. F. and Conway, J. G. (1980) *Lanthanide and Actinide Chemistry and Spectroscopy* (ed. N. M. Edelstein), American Chemical Society, Washington DC, 381–425.
Worden, E. F., Conway, J. G., and Blaise, J. (1985) *Americium and Curium Chemistry and Technology* (eds. N. M. Edelstein, J. D. Navratil, and W. W. Schultz), D. Reidel Publishing Co, 123–34.
Worden, E. F., Conway, J. G., and Blaise, J. (1986) *J. Opt. Soc. Am. B***, 3**, 1092–101.
Worden, E. F., Conway, J. G., and Blaise, J. (1987) *J. Opt. Soc. Am. B,* **4**, 1358–68.
Worden, E. F. (1991–1993) private communications to W. Lauth.
Worden, E. F., Carlson, L. R., Johnson, S. A., Paisner, J. A., and Solarz, R. W. (1993) *J. Opt. Soc. Am. B***, 10**, 1998–2006.
Wyart, J.-F., Kaufman, V., and Sugar, J. (1980) *Phys. Scr.,* **22**, 389–96.
Wyart, J.-F. and Kaufman, V. (1981) *Phys. Scr.,* **24**, 941–52.
Wyart, J.-F. (1998) unpublished calculations.
Wyart, J.-F., Blaise, J. and Worden, E. F. (2005) *J. Sol. State. Chem*., **178**, 589–602.
Wybourne, B. G. (1965) *Spectroscopic Properties of Rare Earths*, John Wiley, New York.
Zalubas, R. and Corliss, C. H. (1974) *J. Res. NBS,* **78A**, 163–246.
Zalubas, R. (1975) *J. Res. NBS,* **80A**, 221–358.